Absolute plate motions in a reference frame defined by moving hot spots in the Pacific, Atlantic, and Indian oceans

Pavel V. Doubrovine,[1,2] Bernhard Steinberger,[1,2,3] and Trond H. Torsvik[1,2,4,5]

Received 1 December 2011; revised 15 June 2012; accepted 25 July 2012; published 11 September 2012.

[1] We defined a new global moving hot spot reference frame (GMHRF), using a comprehensive set of radiometric dates from arguably the best-studied hot spot tracks, refined plate circuit reconstructions, a new plate polygon model, and an iterative approach for estimating hot spot motions from numerical models of whole mantle convection and advection of plume conduits in the mantle flow that ensures their consistency with surface plate motions. Our results show that with the appropriate choice of a chain of relative motion linking the Pacific plate to the plates of the Indo-Atlantic hemisphere, the observed geometries and ages of the Pacific and Indo-Atlantic hot spot tracks were accurately reproduced by a combination of absolute plate motion and hot spot drift back to the Late Cretaceous (~80 Ma). Similarly good fits were observed for Indo-Atlantic tracks for earlier time (to ~130 Ma). In contrast, attempts to define a fixed hot spot frame resulted in unacceptable misfits for the Late Cretaceous to Paleogene (80–50 Ma), highlighting the significance of relative motion between the Pacific and Indo-Atlantic hot spots during this period. A comparison of absolute reconstructions using the GMHRF and the most recent global paleomagnetic frame reveals substantial amounts of true polar wander at rates varying between ~0.1°/Ma and 1°/Ma. Two intriguing, nearly equal and antipodal rotations of the Earth relative to its spin axis are suggested for the 90–60 Ma and 60–40 Ma intervals (~9° at a 0.3–0.5°/Ma rate); these predictions have yet to be tested by geodynamic models.

Citation: Doubrovine, P. V., B. Steinberger, and T. H. Torsvik (2012), Absolute plate motions in a reference frame defined by moving hot spots in the Pacific, Atlantic, and Indian oceans, *J. Geophys. Res.*, *117*, B09101, doi:10.1029/2011JB009072.

1. Introduction

[2] Our ability to reconstruct plate motions in the geologic past has perhaps been one of the most influential tools that shaped the modern views on the evolution of the Earth's lithosphere, providing a quantitative foundation for the theory of plate tectonics [e.g., *McKenzie and Parker*, 1967; *Morgan*, 1968]. Kinematics of relative plate motion can be modeled using marine magnetic anomalies and trends of fracture zones in the world's ocean basins, the oldest of which date back to middle Jurassic time (~170 Ma). Yet, linking the surface plate motion with its ultimate driving force, thermally driven convection in the Earth's mantle, has been a long-standing challenge because of the lack of a suitably defined "absolute" reference frame representative of the entire mantle.

[3] A traditional approach for defining reference frames for absolute plate motion (APM) is based on the use of hot spot tracks [*Wilson*, 1963; *Morgan*, 1971]. A hot spot track is a linear chain of intraplate volcanic edifices, which shows regular progression of eruption ages, often extends to a currently active volcanic center on its younger end, and sometimes can be linked to a Large Igneous Province (LIP) erupted at the older end. *Wilson* [1963] proposed that age progressions and linear geometries of such tracks record motion of lithospheric plates over focused spots of melting fixed in the uppermost mantle (hence the term "hot spot"). *Morgan* [1971] suggested that hot spots are the surface terminations of narrow upwellings of hot material rooted in the lower mantle, which he termed "mantle plumes." These two ideas were pivotal in the subsequent development of hot spot reference frames for absolute plate motion [e.g., *Morgan*, 1981; *Duncan and Clague*, 1985; *Müller et al.*, 1993].

[4] Despite an apparent contradiction between the idea of hot spot fixity and their proposed origin as the 'manifestations of the lower mantle convection' [*Morgan*, 1971, p. 42], it has been argued that motion of plume conduits within the convecting mantle, and motion of hot spots at the surface, are negligibly slow compared to plate motions, so that hot spots could be treated as approximately stationary sources for the purpose of absolute reconstructions [e.g., *Morgan*, 1981; *Duncan*, 1981]. However, it was soon realized that a

[1]Physics of Geological Processes, University of Oslo, Oslo, Norway.
[2]Center for Advanced Study, Norwegian Academy of Science and Letters, Oslo, Norway.
[3]Helmholtz Center Potsdam, GFZ German Research Center for Geosciences, Potsdam, Germany.
[4]Center for Geodynamics, Geological Survey of Norway, Trondheim, Norway.
[5]School of Geosciences, University of Witwatersrand, Johannesburg, South Africa.

Corresponding author: P. V. Doubrovine, Physics of Geological Processes, University of Oslo, PO Box 1048 Blindern, N-0316 Oslo, Norway. (paveld@fys.uio.no)

0148-0227/12/2011JB009072

reference frame defined by fixed hot spots from the Pacific Ocean could not adequately reproduce hot spot tracks in the Indian and Atlantic oceans when reconstructions through the Pacific-Antarctica-Africa chain of relative plate motion (plate circuit) were used to link the Pacific plate to the plates in the Indo-Atlantic hemisphere [*Molnar and Atwater*, 1973]. Similarly, absolute plate motion models based on Indo-Atlantic hot spots were not able to accurately reproduce trends of Pacific tracks [e.g., *Duncan*, 1981; *Molnar and Stock*, 1987]. Although this discrepancy led to some early challenges of hot spot fixity [*Molnar and Atwater*, 1973; *Molnar and Stock*, 1987], a more popular opinion at the time held that, rather than hot spot motion, a reconstruction error within the plate circuit through Antarctica was responsible for the observed inconsistency [e.g., *Duncan*, 1981]. Paleogene extension between West and East Antarctica has been commonly invoked as a likely source of the error in early reconstructions of Pacific-Africa motion (which ignored deformation within Antarctica), and other, more dramatic scenarios have been suggested [*Duncan*, 1981; *Acton and Gordon*, 1994]. Sparse geophysical data coverage of key areas in the southwestern Pacific, and consequently large uncertainties of relative plate rotations in this region [*Cande et al.*, 1995], have provided additional possibilities for the reconstruction error, to the extent that the kinematic models based on the assumption of fixed Pacific and Indo-Atlantic hot spots were deemed more reliable than plate circuit reconstructions [e.g., *Engebretson et al.*, 1985; *Stock and Molnar*, 1988].

[5] Histories of relative plate motion in the southwestern Pacific region have been substantially refined since the mid-1990s [e.g., *Cande et al.*, 1995; *Gaina et al.*, 1998; *Tikku and Cande*, 2000; *Cande and Stock*, 2004a; *Croon et al.*, 2008; *Whittaker et al.*, 2007, also Timing of Kerguelen Plateau formation: Constraints from plate kinematics and triple junction migration, submitted to *Earth and Planetary Science Letters*, 2011; *Williams et al.*, 2011] and now include estimates of Paleogene extension within Antarctica [*Cande et al.*, 2000; *Cande and Stock*, 2004b] and greatly reduced uncertainties. Still, reexaminations of the Pacific plate circuit reconstructions using updated kinematic solutions show that it is not possible to fit hot spot tracks globally (in the Pacific, Atlantic and Indian oceans) while assuming hot spot fixity and simultaneously maintaining integrity of the global plate circuit [*DiVenere and Kent*, 1999; *Raymond et al.*, 2000; *Steinberger et al.*, 2004; *Doubrovine and Tarduno*, 2008a, 2008b].

[6] Paleomagnetic data from the Pacific plate provide further evidence against hot spot fixity [e.g., *Tarduno and Gee*, 1995; *Tarduno et al.*, 2003]. Notably, studies of basalts drilled from the Emperor seamounts [*Tarduno and Cottrell*, 1997; *Tarduno et al.*, 2003; *Doubrovine and Tarduno*, 2004] documented approximately 14° (~1500 km) of southward motion of the Hawaiian hot spot in Late Cretaceous through early Eocene time (81–47 Ma), in the direction and at a rate that are not compatible with estimates of true polar wander (TPW) [*Besse and Courtillot*, 2002; *Tarduno*, 2007; *Steinberger and Torsvik*, 2008]. Geodynamic models for the motion of Hawaiian plume conduit consistently predict dominantly southward hot spot motion and the overall amount of latitudinal displacement comparable with paleolatitudes recorded by the Emperor seamounts [*Steinberger and O'Connell*, 1998; *Steinberger*, 2000; *Steinberger and Antretter*, 2006]. Thus, the rapid southward drift of the Hawaiian hot spot during Late Cretaceous-Paleogene time can be sensibly interpreted as a result of advection of the plume conduit by the ambient flow of convecting mantle [*Tarduno*, 2007; *Tarduno et al.*, 2009].

[7] Large-scale relative motion between the Pacific and Indo-Atlantic hot spots suggested by the analysis of plate circuits and paleomagnetic data precludes the use of globally fixed hot spots as an absolute reference frame. On the other hand, reasonable fits to hot spot tracks can be obtained if the Pacific and Indo-Atlantic hot spots are treated separately, i.e., by assuming that hot spots within each group have not moved relative to each other, but at the same time allowing motion between the two groups. This situation has led to a real dichotomy of fixed hot spot reference frames, which are based either exclusively on Pacific hot spots [*Duncan and Clague*, 1985; *Koppers et al.*, 2001; *Andrews et al.*, 2006; *Wessel and Kroenke*, 1997], or on Indo-Atlantic hot spots [*Morgan*, 1981; *Müller et al.*, 1993]. Although some studies argued that the Indo-Atlantic hot spots have been approximately fixed since the Late Cretaceous [e.g., *O'Neill et al.*, 2005], the use of hot spots from only one hemisphere raises concerns whether such reference frames are fully suitable for representing the entire mantle.

[8] The recognition of hot spot mobility during the last decade led to the emergence of a new class of absolute reference frames based on moving hot spots [*Steinberger et al.*, 2004; *O'Neill et al.*, 2005; *Steinberger and Gaina*, 2007; *Torsvik et al.*, 2008]. The approach pioneered by *Steinberger et al.* [2004] utilizes the modeling technique of *Steinberger and O'Connell* [1998] for estimating hot spot motions from numerical results on the advection of plumes in the large-scale mantle flow field. Absolute plate motions are defined in a way similar to the fixed hot spot reconstructions (i.e., by fitting the geometries and age progressions along the hot spot tracks), but with the past hot spot locations varied through time as predicted by the numerical model. This approach showed qualitatively better performance in fitting hot spot tracks globally [*Steinberger et al.*, 2004; *Torsvik et al.*, 2008]. However, because the reconstruction uncertainties were not estimated in these studies, it is not possible to test whether the global hot spot fits of *Steinberger et al.* [2004] and *Torsvik et al.* [2008] are statistically acceptable. Only a few studies provided rigorous uncertainty analysis of absolute plate rotations relative to hot spots [*Harada and Hamano*, 2000; *O'Neill et al.*, 2005; *Andrews et al.*, 2006; *Wessel et al.*, 2006], but none of them attempted to fit hot spot tracks globally.

[9] In the remainder of the paper, we will use the terms "absolute plate motion," "plume motion" and "hot spot motion" to refer to the motions of lithospheric plates, mantle plumes and hot spots in a reference frame defined by moving hot spots. Practically, the moving hot spot reference frame corresponds to a "mean mantle" reference frame, in which the convective motions withing the mantle have been averaged to no net rotation [*Steinberger and O'Connell*, 1998; *Steinberger*, 2000]; hence, it can be used as a proxy for the entire solid Earth. Fixed hot spot models will be treated as a specific case, in which plumes and hot spots are assumed to remain stationary in the mean mantle reference frame. Finite rotations that reconstruct positions of lithospheric plates in

moving or fixed hot spot reference frames will be referred to as "absolute rotations" to distinguish them from kinematic parameters describing relative plate motions.

[10] This study presents a new generation of the global moving hot spot reference frame (GMHRF), in which we combined updated plate circuit reconstructions, radiometric age data from hot spot tracks, and numerical estimates of hot spot motion to produce a fully self-consistent model for absolute plate kinematics. We estimated uncertainties of absolute plate rotations and evaluated the goodness of fit through formal statistical tests based on spherical regression analysis [*Chang*, 1986, 1987]. We examined alternative plate circuits that can be used to reconstruct the Pacific plate relative to the plates of the Indo-Atlantic hemisphere back to Late Cretaceous time (83.5 Ma) [*Doubrovine and Tarduno*, 2008a, 2008b] and discussed their implications for the overall quality of kinematic models based on moving hot spots. To further test the hypothesis of global hot spot fixity, we compared the quality of fit obtained in the moving and fixed hot spot models with the identical error budgets. Our results provide a new kinematic framework, in which we defined revised histories of absolute motion for the African and several other major lithospheric plates, and derived estimates of net lithosphere rotation and true polar wander (TPW) since Early Cretaceous time (~120 Ma).

2. Building Blocks of a Moving Hot Spot Reference Frame

[11] There are three key elements that define a moving hot spot reference frame: (1) ages and geometries of hot spot tracks, (2) relative plate motions, and (3) motions of mantle plumes. This section discusses the choices we made in selecting parameters for numerical models and input data for fitting absolute rotations.

2.1. Hot Spot Tracks

[12] Two hot spot tracks on a single plate are sufficient to calculate its absolute motion, whereas using a single track creates an under-determined problem with multiple solutions [cf. *Andrews et al.*, 2006]. For instance, using the Hawaiian and Louisville tracks on the Pacific plate, or Tristan and Reunion tracks on the African plate, it is possible to estimate the absolute motions for these two plates directly from their native tracks. However, previous work [*Steinberger et al.*, 2004] showed that optimizing fits to hot spot tracks in the Pacific Ocean produces absolute plate motion models that do not accurately reproduce Indo-Atlantic hot spot tracks, and vice versa. Uncertainties associated with modeled plume motions (section 2.3) are typically large compared to the errors in relative plate reconstructions (section 2.2). These unrecognized errors can significantly bias absolute plate kinematics when it is based on a small number of tracks from a single plate. In contrast, when a large number of tracks evenly distributed around the globe are fitted, we would expect the individual biases to average out, resulting in a more reliable APM model.

[13] Although some fifty hot spots have been described in the literature (see, for example, compilations of *Morgan* [1981] and *Steinberger* [2000]), and several were suggested to be sourced by deep mantle plumes, essentially rising from the core-mantle boundary (CMB) [*Courtillot et al.*, 2003], only few of them feature well-defined tracks with clearly documented progressions of volcanic ages that could provide sensible input for defining absolute plate motions. In our analysis, we have restricted ourselves to arguably the best-studied tracks of five archetypal hot spots: the Hawaiian and Louisville hot spots in the Pacific Ocean, and Tristan, Reunion and New England in the Indo-Atlantic hemisphere. All of them satisfy the criteria of *Courtillot et al.* [2003] indicative of their "primary" origin in the deep mantle. Radiometric ages of dated volcanic edifices along the hot spot tracks were collected from the literature, mostly following the compilations of *Steinberger* [2000], *Steinberger et al.* [2004], and *O'Neill et al.* [2005], and using updated ages that became recently available for the Pacific tracks [*Sharp and Clague*, 2006; *Duncan and Keller*, 2004; *Koppers et al.*, 2004, 2011]. The complete list of dated locations and ages is provided in the auxiliary material (Table S1).[1]

2.2. Relative Plate Motions

[14] Incorporating data from hot spot tracks formed on different plates into a common reference frame requires estimates of relative plate motion. Practically, this is done by reconstructing coeval locations from all tracks that are present at a certain age relative to a selected "anchor" plate. The reconstructed locations correspond to the paleo-positions of hot spots in the reference frame of the anchor plate, providing a means for calculating the absolute displacement of the anchor plate since the age of reconstruction (this will be fully described in section 3). Absolute rotations for the remaining plates can then be calculated by adding relative plate motions to the absolute rotations of the anchor plate.

[15] Relative plate motions can be accurately reconstructed by matching marine magnetic anomalies and fracture zones created by seafloor spreading between adjacent plates separated by a mid-ocean ridge, using formal statistical approaches for estimating best-fit rotations and their uncertainties [e.g., *Hellinger*, 1981; *Chang*, 1988]. In cases when two plates do not share a common spreading ridge boundary, their relative motions are estimated by combining rotations in a chain of relative plate motion (plate circuit), i.e., by simultaneous reconstruction of several plates separated by intervening mid-ocean ridges. Because the African plate has been traditionally used as a reference plate in hot spot reconstructions [e.g., *Müller et al.*, 1993], we compiled finite rotations for reconstructing motion of the North American, South American, Somalian, Indian and Pacific plates relative to south Africa using published kinematic models and appropriate plate circuits. Absolute reconstruction ages were assigned using identifications of marine magnetic anomalies according to the geomagnetic polarity timescales of *Cande and Kent* [1995] for Late Cretaceous and Cenozoic, and of *Gradstein et al.* [1994] for Early to Late Cretaceous time; the switch-point between the two scales was set to the younger boundary of the Cretaceous Normal Superchron (CNS) at 83.5 Ma following *Torsvik et al.* [2008]. For combining finite rotations in plate circuit reconstructions, we used the procedure described in *Doubrovine and Tarduno* [2008a], which involves necessary interpolations between finite rotations

[1]Auxiliary material data sets are available at ftp://ftp.agu.org/apend/jb/2011jb009072. Other auxiliary material files are in the HTML. doi:10.1029/2011JB009072.

of the original plate-pair kinematic models to produce a common set of reconstruction ages for all individual reconstructions involved in a plate circuit. Wherever rotation uncertainties were available from the original kinematic models, they were propagated though plate circuits and the uncertainties of combined rotations were estimated using the formulations of *Doubrovine and Tarduno* [2008a].

[16] Our selection of rotation parameters for individual plate-pair reconstructions closely follows a recent compilation of *Torsvik et al.* [2008]. In cases when updated kinematic solutions were available, we have modified the relative plate motion model. These modifications include (1) the estimates of Neogene extension within the African plate (Somalia-Nubia motion) due to the opening of the East African Rift system, (2) updated Cenozoic reconstructions of the Indian Ocean basin, and (3) revised plate circuit models for the Pacific plate motion as described below. The sources of all remaining reconstructions have been referenced in *Torsvik et al.* [2008].

[17] The extension across the East African Rift system, which separated the African plate into the Nubian and Somalian plates during Neogene time, has been recorded by the marine magnetic anomalies formed at the Southwest Indian Ridge, in the Red Sea and the Gulf of Aden [e.g., *Chu and Gordon*, 1999; *Lemaux et al.*, 2002]. *Molnar and Stock* [2009] argued that active rifting began at ~11 Ma (i.e., at chron C5o time), and we used the rotation parameters of *Horner-Johnson et al.* [2007] and *Lemaux et al.* [2002] to reconstruct the Somalia-Nubia motion since that time. Prior to 11 Ma (back to Late Cretaceous time, 83.5 Ma), the African plate was treated as a single, rigid plate. Noting that the Somalia-Nubia rotations are small (the overall amount of displacement is of the order of few tens of kilometers) and could have been neglected compared to the intrinsic uncertainties of hot spot locations, we nevertheless chose to include them and reconstruct the Somalian part of the Reunion track with respect to south Africa.

[18] The India-Africa motion was reconstructed using the India-Somalia-Nubia and India-Capricorn-Somalia-Nubia plate circuit models that combine updated kinematic parameters for the opening of the Indian Ocean basin during the Cenozoic [*Merkouriev and DeMets*, 2006; *DeMets et al.*, 2005; *Cande et al.*, 2010]. The India-Somalia rotations have been tabulated in a recent study of *van Hinsbergen et al.* [2011]. For the upper Late Cretaceous reconstructions (65–83.5 Ma), we used the India-Somalia rotations of *Molnar et al.* [1988], and prior to 83.5 Ma, the Indian plate motion was calculated using the India-Madagascar-Africa plate circuit of *Torsvik et al.* [2008].

[19] Motion of the Pacific plate relative to the African (Nubian) plate since Late Cretaceous time (chron C34y, 83.5 Ma) was reconstructed using two alternative kinematic models [*Steinberger et al.*, 2004; *Doubrovine and Tarduno*, 2008a, 2008b]. The first model (which will be referred to as the "Antarctic plate circuit") combines the reconstructions of the Pacific plate relative to West Antarctica (Mary Byrd Land), West Antarctica relative to East Antarctica, and East Antarctica relative to south Africa. The second model uses the reconstructions of Campbell Plateau (which has been a part of the Pacific plate since the Late Cretaceous) relative to the Lord Howe Rise, the Lord Howe Rise to Australia, Australia to East Antarctica, and East Antarctica to Africa. In the remainder of the paper, we will refer to this model as the "Australian plate circuit." The individual reconstructions involved in the two plate circuit models have been described in detail in *Doubrovine and Tarduno* [2008a, 2008b], and here we retained their choices for the finite rotations defining relative plate motions in the southwestern Pacific ocean. The only modification that has been made is the use of detailed reconstructions of the Pacific-West Antarctica motion since middle Eocene time (chron C20o, 43.8 Ma) recently published by *Croon et al.* [2008]. Similarly to *Steinberger et al.* [2004] and *Doubrovine and Tarduno* [2008a], we switched from the reconstructions through the Australian plate circuit for times older than chron C21y (46.3 Ma) to those using the Pacific-West Antarctica-East Antarctica connection for times younger than chron C20o (43.8 Ma), and interpolated rotations for times between chrons C21y and C20o. For times younger than chron C20o, the two plate circuit models are identical. The rotation parameters of *Royer and Chang* [1991] and *Bernard et al.* [2005], describing the motion between East Antarctica and Africa since Late Cretaceous time, were used for the final link in both plate circuits.

[20] Whereas the histories of relative plate motion are well established from geophysical data collected in the Indian and Atlantic oceans, larger uncertainties exist for reconstructions linking the Pacific plate with the plates of Indo-Atlantic realm. Specifically, the record of seafloor spreading between West and East Antarctica is limited to the area flanking the Adare Trough in the western Ross Sea, which led to large uncertainties of the estimated West–East Antarctica rotations [*Cande et al.*, 2000; *Cande and Stock*, 2004b]. Extrapolations and considerations of plate circuit closure were used to derive the East–West Antarctica rotations for reconstruction ages older than chron C13o time (33.5 Ma) [*Cande et al.*, 2000]. The fit of rifted margins of the Lord Howe Rise and Campbell Plateau [*Sutherland*, 1995] is subject to similarly large uncertainties.

[21] Two competing models have been proposed for the early opening between Australia and East Antarctica in Late Cretaceous to Paleocene time [*Tikku and Cande*, 2000; *Whittaker et al.*, 2007, 2010, also submitted manuscript, 2011; *Williams et al.*, 2011], a period of very slow spreading at the Southeast Indian Ridge with no clearly identifiable fracture zones. The reconstruction of *Tikku and Cande* [2000] suggests nearly steady, north–south oriented motion between Australia and East Antarctica during this interval, producing a tight fit between the Broken Ridge and Kerguelen Plateau (the two oceanic plateaus are conjugate features separated in middle Eocene time, ~40 Ma), but also causes an overlap of Tasmania and the South Tasman Rise with East Antarctica in the Late Cretaceous. In the alternative scenario proposed by *Whittaker et al.* [2007], the initial Australia-Antarctica opening was oblique, in a northwest–southeast direction, changing to the north–south motion in early Eocene time (~50 Ma). This reconstruction eliminates the Tasmania-Antarctica overlap in the Late Cretaceous and results in a sensible juxtaposition of old geologic terranes of Australia and Antarctica, but at the same time opens a gap between the Broken Ridge and Kerguelen Plateau [*Tikku and Direen*, 2008]. To address this inconsistency, *Whittaker et al.* [2010, also submitted manuscript, 2011] and *Williams et al.* [2011] revised their rotation parameters, suggesting strike-slip motion between the two oceanic plateaus in the Late

Table 1. Present Locations and Ages of Hot Spots

Hot Spot	Lat. (°N)	Lon. (°E)	Age (Ma)
Hawaii	19.4	−155.3	120
Louisville	−50.9	−138.1	120
New England	29.3	−29.1	125
Reunion	−21.2	55.7	66
Tristan	−38.7	−11.3	132

Cretaceous. Recognizing that neither model completely resolves all complexities of the early Australia-Antarctica rifting history, we tried both sets of rotation parameters in reconstructions of the Pacific plate motion through the Australian plate circuit. The solutions obtained with the rotations of *Tikku and Cande* [2000] and Whittaker et al. (submitted manuscript, 2011) will be referred to as the Australian plate circuit models 1 and 2, respectively.

2.3. Plume Motions

[22] Hot spot tracks formed on a lithospheric plate by its motion over the underlying hot spot sources record both the absolute displacement of the plate and motions of plumes entrained into the mantle flow. To separate the contribution of absolute plate motion from this combined signal, motions of plume conduits have to be estimated independently. This can be done through numerical modeling of whole mantle convection and advection of plume conduits into the mantle flow field [*Steinberger and O'Connell*, 1998; *Steinberger*, 2000].

[23] Present locations and ages of the five hot spots that we have modeled are listed in Table 1; these closely follow the compilation of *Steinberger and Antretter* [2006]. The locations of Hawaiian, Reunion and Tristan hot spots are based on observations of active and recent hot spot-related volcanism. For the Tristan hot spot, we assumed the present location between Tristan da Cunha and Gough islands, both of which have been active recently. For the New England and Louisville hot spots, no recent volcanism has been documented, and their present positions were assigned using the locations of the youngest seamounts in these chains: seamount 18 of the Great Meteor group for the New England hot spot [*Tucholke and Smoot*, 1990], and the "138.1°W" seamount of the Louisville track [*Lonsdale*, 1988]. Present locations ∼200–350 km south of the 138.1°W seamount have been also proposed for the Louisville hot spot from reconstructions of the Pacific plate relative to the fixed hot spots [*Wessel and Kroenke*, 1997; *Raymond et al.*, 2000; *Wessel et al.*, 2006; *Wessel and Kroenke*, 2008]. Because these estimates may be significantly biased by unaccounted hot spot motions, we did not consider them suitable for our analysis.

[24] The ages of Louisville, Reunion and Tristan hot spots were assigned using the radiometric estimates from the associated LIPs (Ontong Java-Manihiki-Hikurangi, Deccan and Parana-Etendeka LIPs, respectively). We note that the assumption that the formation of ∼120-Ma-old Ontong Java, Manihiki and Hikurangi plateaus [*Taylor*, 2006] was related to the arrival of the Louisville plume head underneath the lithosphere of the paleo-Pacific ocean is questionable because the older segment of the Louisville track has been subducted beneath the Tonga trench. Although we could not rule out a younger age of the hot spot (between 120 and 80 Ma), we preferred to keep the 120 Ma assignment because of a possible temporal association with the widespread Aptian pulse of volcanic activity in the western Pacific, traditionally attributed to a mantle plume (see *Doubrovine et al.* [2009] and references therein for discussion). A recent study of *Chandler et al.* [2012] showed that the reconstructions of the Ontong Java-Manihiki-Hikurangi LIP using the hot spot reference frames of *O'Neill et al.* [2005], *Wessel and Kroenke* [2008] (WK08-A) and a modification of the latter (WK08-D), which allowed motion of the Hawaiian hot spot during the formation of the Emperor seamounts (83.5–47 Ma), consistently placed the igneous province 8° to 19° north to northeast of the recent position of the Louisville hot spot. Nevertheless, because of the large area of the LIP (∼5 × 10^6 km^2) and potentially large uncertainties in all APM models for the Pacific plate for ages greater than 83.5 Ma, *Chandler et al.* [2012] concluded that the connection between the Ontong Java-Manihiki-Hikurangi LIP and the Louisville hot spot remains a viable hypothesis.

[25] The New England track is not linked to a LIP, and we assigned the age using the oldest radiometric dates from the volcanics produced by this hot spot (Cretaceous rocks of White Mountains Series and Monteregian Hills [see *van Fossen and Kent*, 1992, and references therein]). The older part of the Hawaiian track has been subducted at the Kuril-Aleutian trench and the age of the hot spot is uncertain. Following *Steinberger and Antretter* [2006], we assumed a 120 Ma initiation age for the Hawaiian hot spot.

[26] The global mantle flow field and its variations through time were modeled using the spectral method originally developed by *Hager and O'Connell* [1979, 1981]. The flow was computed within a spherical shell and was modeled as driven by mantle density heterogeneities with plate velocities imposed as a boundary condition at the surface, the free-slip condition at the core-mantle boundary, and a radial viscosity structure within the mantle. Because the numerical flow model does not consider lateral viscosity variations, the calculated flow field does not feature net rotation of the lithosphere relative to the mantle. Hence, absolute plate velocities had to be modified such that net lithosphere rotation was zero. This modification was necessary in order to compute the mantle flow and hot spot motions in the mean mantle reference frame (i.e., without net rotation of the entire mantle). However, when fitting absolute plate rotations (section 3), net rotation of the lithosphere was not assumed to remain zero. This is equivalent to artificially introducing net rotation of the lithosphere relative to the mantle, as has been discussed by *Mihalffy et al.* [2008].

[27] The mantle was treated as an incompressible viscous liquid with phase transitions as in the study of *Steinberger* [2000]. The present-day mantle density structure was inferred from the SMEAN seismic tomography model of *Becker and Boschi* [2002], using the depth-dependent velocity to density scaling factors of *Steinberger and Calderwood* [2006] and reference density and seismic velocity values from the preliminary reference Earth model (PREM) [*Dziewonski and Anderson*, 1981]. Density variations above the depth of 220 km were set to zero to exclude lithospheric effects. The preferred model of *Steinberger and Calderwood* [2006] (model 2b) was used for the radial variation of mantle viscosity; this viscosity model is constrained by mineral physics data and surface observations (geoid and heat flux). The

inferred present density anomalies were advected back in time in the calculated flow field at 1 Ma increments following the approach of *Steinberger and O'Connell* [1998], which is based on approximating the temporal variation of density by the contribution due to advection alone, i.e., ignoring all other terms in the equation of heat transfer (heat diffusion, heat production, viscous dissipation). This is a valid approximation for reconstructing the mantle density structure over timescales up to ~70 Ma, at which thermal diffusion is small compared to the advective heat transport [*Steinberger and O'Connell*, 1998]. However, for reconstructions beyond 70 Ma, severe numerical artifacts can develop in the backward advection calculations [e.g., *Conrad and Gurnis*, 2003]. Hence, we chose to limit the backward advection in our plume advection experiments to 70 Ma, and for the older times (up to ~130 Ma) we assumed a constant flow field defined by the density structure reconstructed at 70 Ma. This simplification creates additional uncertainty for the modeled hot spot motions.

[28] Plume motions were calculated using the algorithm of *Steinberger and O'Connell* [1998], which discretizes a plume conduit into a finite number of segments and assumes that the total velocity of each segment is the sum of the mantle flow velocity at the segment midpoint and the plume vertical buoyant rising velocity. Conduits were modeled as initially vertical, originating from the top of the low-viscosity D″ layer above the CMB (at the depth of ~2620 km) and terminating at the bottom of the lithosphere (the 100 km average depth was used). The initial geometry corresponds to the hot spot ages listed in Table 1. Present conduit geometries were calculated by forward advection of plumes in the flow field computed as described above. The bases of conduits were kept at their original depth (2620 km) and were allowed to move with velocities defined by the horizontal flow component at that level. The initial positions of plumes were estimated using an iterative procedure, by matching the present-day hot spot locations with the coordinates of the upper terminations of advected conduits [*Steinberger*, 2000]. For a detailed description of the numerical model and plume parameters used in our calculations, see the reference case of *Steinberger and Antretter* [2006].

3. Reconstruction Method

[29] The workflow for defining a moving hot spot reference frame is summarized in Figure 1. First, the locations corresponding to the selected reconstruction ages were identified in hot spot tracks from the available radiometric data (section 2.1) and reconstructed relative to a reference (anchor) plate using relative plate rotations (section 2.2). Hot spot motions in the mantle reference frame were modeled using the numerical technique described in section 2.3. Spatial uncertainties were assigned to the reconstructed track locations and the coeval positions of hot spots (section 3.1), which were then used as the input for the spherical regression algorithm to estimate the absolute rotations of the anchor plate and their uncertainties (section 3.2). The control step was to test whether the fitted rotations reconstruct the track locations onto their respective hot spots within the errors assigned to the input data through a formal test for the goodness of fit (section 3.2). Relative plate motions were combined with absolute motions of the anchor plate to calculate the absolute rotations for all remaining plates. This generated a new global absolute plate kinematic model that would generally predict slightly different hot spot motions. In order to produce an internally consistent APM model, the calculations of global mantle flow and advection of plumes were repeated with the newly defined kinematic solution until the differences between the absolute plate motions produced in successive iterations became negligible (section 3.3).

[30] Our reconstruction method (section 3.2, Appendix A) required *a priori* known uncertainties of input data. An alternative approach for defining uncertainties of fitted rotations would be assuming that the assigned data errors are only *relatively correct* and estimating the unknown data variances from the model misfit. This approach, however, does not provide a quantitative way to evaluate the quality of obtained fit, or discriminate between alternative models with identical error budgets (e.g., when the tracks are reconstructed through different plate circuits, section 4). In essence, when data errors are deduced from the misfit, the uncertainties of fitted rotations become as large as necessary to capture any misfit within the model error, no matter how bad the misfit is. Hence, similarly to *Andrews et al.* [2006], we chose to assign the errors to the past hot spot and track locations and treated them as known values. As discussed further in section 3.1, the assigned errors were realistic in the sense that they neither grossly overestimated nor underestimated uncertainties conceivable for our data selection.

3.1. Input Locations and Assigned Errors

[31] Similarly to the study of *O'Neill et al.* [2005] and many others, we used (south) Africa as a reference or anchor plate and fitted its absolute rotations at 10 Ma increments back to Late Cretaceous time (80 Ma) using hot spot tracks from the Pacific, Atlantic and Indian oceans. Further back in time, we also estimated absolute rotations for 100 and 124 Ma; these however were based on the Atlantic tracks only (Tristan and New England hot spots).

[32] Because the available radiometric ages (section 2.1 and auxiliary material Table S1) were limited by the distribution of the sampling sites, a necessary preprocessing step for using age progressions and geometries of the tracks was to estimate the positions corresponding to the selected reconstruction times. Here we chose to approximate the actual tracks by spherical splines with a smoothing parameter varying between 500 and 2000 [*Jupp and Kent*, 1987], using the dated localities as the input and weighting them according to the uncertainties of age estimates. The smoothing parameter controls the trade-off between the smoothness of the spline curve and the accuracy of approximation. Smaller values tend to produce fitted curves that closely follow the data points, but exhibit large variations in curvature. Higher values reduce the curvature variation by allowing larger departures of the curve from the data. In the limiting cases, the spherical spline with a zero smoothing parameter strictly interpolates the data points, whereas as the smoothing parameter approaches infinity, the spline curve tends toward a great circle segment.

[33] We applied the following criteria for selecting appropriate values of the smoothing parameter: (i) the spline curves should accurately represent the geometries of hot spot tracks, (ii) the ages along the smoothed curves should increase

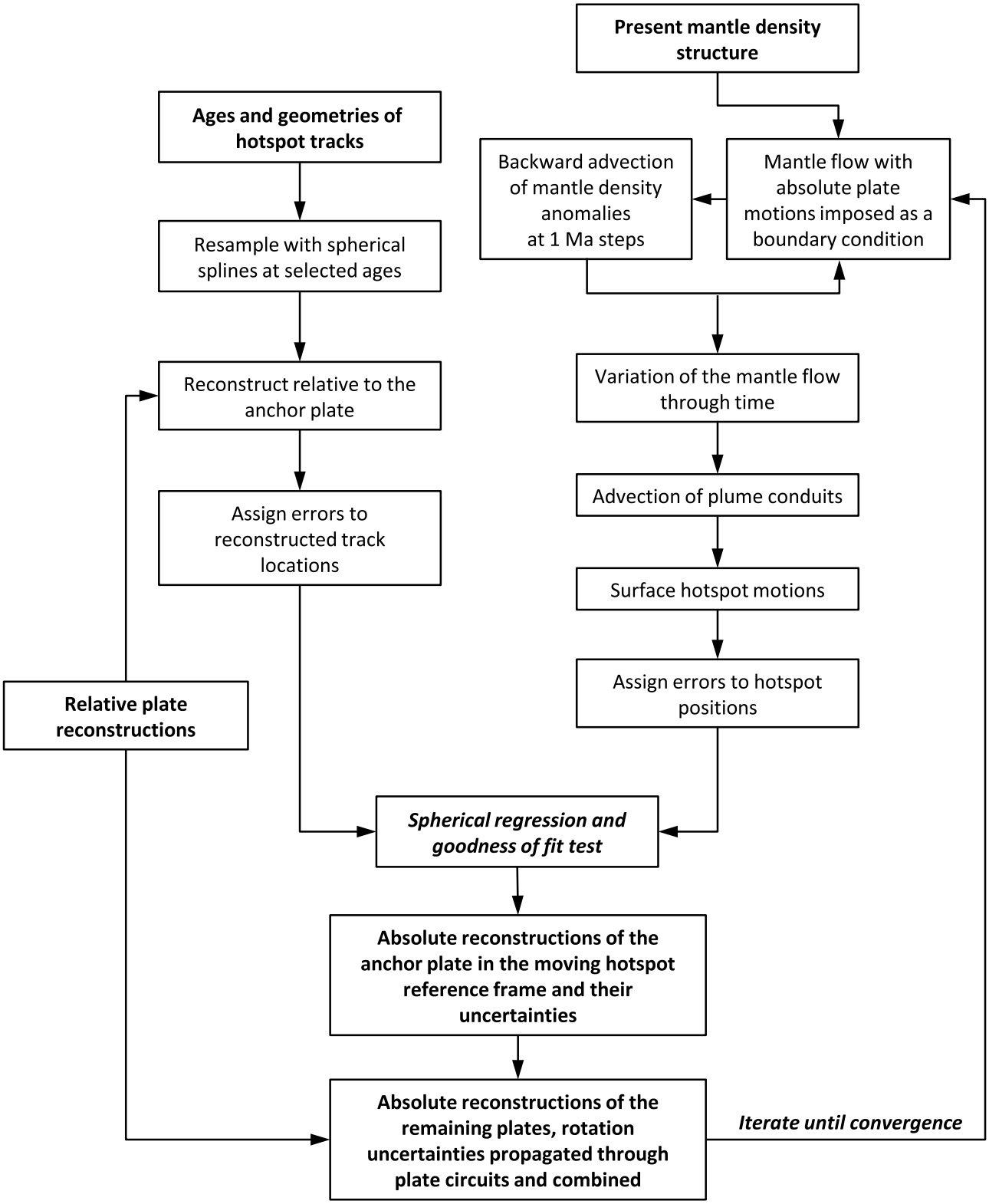

Figure 1. A flowchart illustrating the steps involved in building a moving hot spot reference frame (see text for description).

monotonically with the increasing distance from the hot spot, and (iii) the root mean square (RMS) misfit between the dated locations projected on the spline curve and the points of the spline corresponding to their ages should not exceed 150 km, which is the lower limit for the spatial uncertainty typically assigned to the spline-approximated positions along tracks.

[34] Spline curves were used to resample tracks at 10 Ma increments (e.g., Figure 2). Circular uncertainties (at a nominal

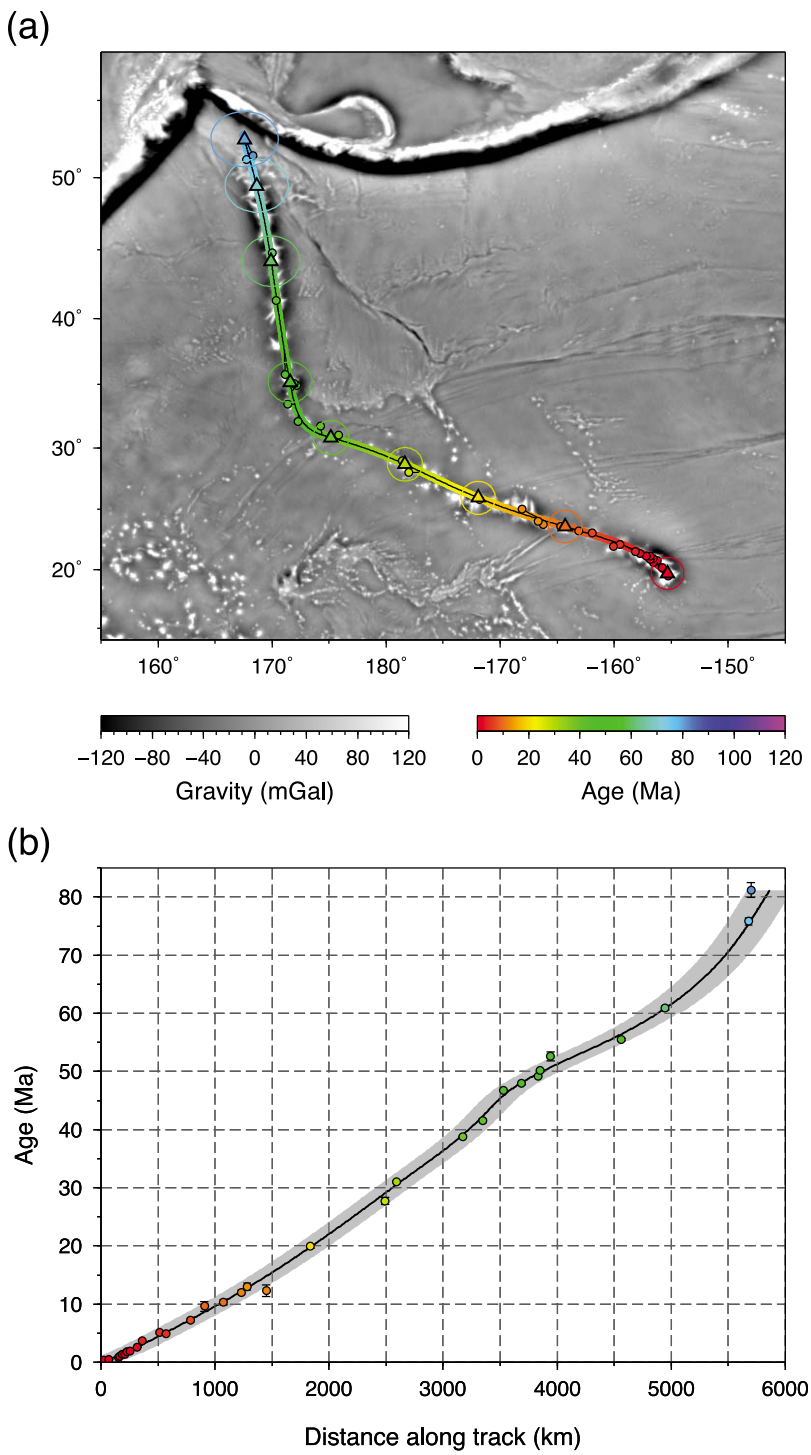

Figure 2. (a) An example of the smoothing spherical spline (smoothing parameter = 500) fitted to the age data for the Hawaiian hot spot track. Triangles show the positions on the spline curve sampled at 10 Ma increments. Circles are the 95% uncertainties assigned to the spline locations. Small dots with tie-lines to the spline are the locations of radiometrically dated samples. Marine gravity anomaly map is from *Sandwell and Smith* [1997]. Miller cylindrical projection. (b) Ages of dated localities as a function of their distance along the track from the Hawaiian hot spot (circles). Black curve shows the age-distance progression for the spline model; gray band around this curve corresponds to the 95% uncertainties regions assigned to spline points.

95% confidence level) were assigned to spline-interpolated positions based on the distribution of the dated localities and their observed ages relative to the spline curves. For example, 150 km uncertainties were assigned to the 0–40 Ma locations along the Hawaiian hot spot track, a 175 km uncertainty was set for the 50 Ma position, and a 200 km uncertainty was assigned to the 60–80 Ma locations. Figure 2 shows that the spherical spline produced an excellent fit for the geometry of the Hawaiian-Emperor chain and the simple error model adopted for the resampled points captured the variation of the observed ages relative to the spline model. A similar approach was used for approximating the remaining tracks. For the Reunion track, a 150 km uncertainty was assigned for the 0–40 Ma locations, and a 200 km error was set for the 50–60 Ma locations. For the Tristan, New England, and Louisville hot spots, whose present-day locations are less certain (section 2.1), a 200 km uncertainty was assigned for all positions. The RMS misfits between the dated locations projected onto the model curves and spline positions corresponding to their ages were less than 90 km for the Hawaiian, Louisville, New England and Reunion tracks, and ~140 km for the Tristan track, indicating that the spherical splines provided a close fit to the observed age progressions.

[35] Assigning uncertainties to the past hot spot locations calculated through numerical modeling of the mantle flow and plume conduit advection (section 2.3) was less straightforward, as has been discussed in the earlier studies [e.g., *Steinberger et al.*, 2004; *O'Neill et al.*, 2005]. Specifically, *O'Neill et al.* [2005] noted that 'the physical uncertainties in the input to these calculations, together with the uncertainties in modeling parameters, make it difficult to constrain the uncertainties in these calculated positions in any meaningful way.' From the analysis of a large number of models, they found that (i) the uncertainty of hot spot motion (arising from the uncertainties of model parameters) is generally similar to the amounts of motion itself, (ii) increases with age, and (iii) the uncertainty region for a calculated past hot spot location usually overlaps with its present-day uncertainty region. Based on these findings, we devised a simple error model for the calculated hot spot locations, by using the present-day uncertainties assigned to hot spots (150 km for Hawaii and Reunion, and 200 km for Tristan, New England and Louisville) and increasing it with age at a rate of 2.25 km/Ma (e.g., 180 km in 80 Ma). We note that although this simple error model probably underestimated true uncertainties for the ages older than 40 Ma, we nevertheless preferred to use the "tighter" confidence regions because doing so did not introduce unnecessary large uncertainties to the fitted rotations (section 4). Notice, however, that the assigned errors (both for the locations along tracks and for the modeled positions of hot spots) should be viewed only as first-order approximations of the true data variances; hence we chose to defer rejection of the models that failed the formal goodness of fit test (section 3.2) in cases of marginal significance.

3.2. Spherical Regression

[36] In studies of relative plate motion, a statistically rigorous regression technique for fitting finite rotations and analyzing their uncertainties has been developed and routinely used over the last two decades [*Hellinger*, 1981; *Chang*, 1988; *Chang et al.*, 1990] . In contrast, various methods have been proposed for estimating absolute plate rotations in hot spot reconstructions, and no single modeling approach has yet been fully accepted by the geophysical community as a standard technique. The traditional approach [e.g., *Morgan*, 1981; *Duncan and Clague*, 1985] is based on fitting coeval segments of hot spot tracks by small circles about a stage rotation pole, and using their lengths and age estimates to derive the angular rate of absolute motion. The most important shortcomings of this technique, which limit its use for the purposes of our study, are that it assumes fixed hot spots and does not provide a straightforward way for estimating rotation uncertainties; other limitations have been discussed by *Wessel et al.* [2006].

[37] Several recent studies explored possibilities for quantifying uncertainties in hot spot reconstructions. *Harada and Hamano* [2000] and *Wessel et al.* [2006] developed a technique for fixed hot spot reconstruction, which uses a grid search in the Euler pole latitude-longitude space to define all possible candidate rotations that are consistent with the observed geometries of hot spot tracks within a wide range of rotation angles. Using available radiometric dates, the candidate rotations are binned into groups that correspond to selected reconstruction ages. A mean rotation and its uncertainty (covariance matrix) are then estimated from the population of rotations within each group.

[38] *Andrews et al.* [2006] adopted a numerical approach for solving a least squares regression problem of finding a rotation that minimizes the misfit between two sets of points on the sphere (current hot spots positions and coeval locations on their respective tracks). The uncertainties of fitted rotations are estimated from the errors assigned to the data points, allowing a formal statistical test for the goodness of fit. This method was originally intended for testing fixed hot spot models, but its application is not limited to the case of fixed hot spots.

[39] *O'Neill et al.* [2005] used a modification of the *Hellinger* [1981] criterion of fit and formulations of *Chang* [1988] to determine absolute rotations in the Indo-Atlantic moving hot spot reference frame and their uncertainties. However, the method of *Chang* [1988] was specifically designed for estimating rotations from plate boundary crossings and is not a natural solution for the regression problem relevant to hot spot reconstructions. A simpler, yet statistically rigorous technique for fitting two sets of spherical data was developed by *Chang* [1986, 1987], and we used these formulations to define finite rotations, estimate their uncertainties and test for the goodness of fit in our moving hot spot reconstructions. Our approach is similar to the method of *Andrews et al.* [2006] in the way we defined a criterion of fit and derived a goodness of fit statistic from the assigned data errors, but uses an analytical solution for the least squares regression problem. It also shares similarities with the *O'Neill et al.* [2005] method in the way we treated and analyzed rotation uncertainties. The essential definitions and formulations used in our analysis are summarized in Appendix A; a detailed discussion, derivations and mathematical proofs can be found in the original works of *Chang* [1986, 1987].

[40] For each reconstruction age, we estimated the best-fit finite rotation $\hat{A}$ that reconstructs the anchor plate (Africa) to its position relative to the moving hot spots at that age. The rotation uncertainty was expressed as a covariance matrix of

a small rotation pseudo-vector **h**, which relates the estimated rotation to its "true" unknown value A_0 through the equation

$$\hat{A} = A_0\Phi(\mathbf{h}) \tag{1}$$

where $\Phi(\mathbf{h})$ denotes the right-hand rule rotation about vector **h** by $|\mathbf{h}|$ radians. Although **h** is unknown, its covariance matrix, $\mathrm{cov}(\mathbf{h}) = \mathrm{E}(\mathbf{h}\mathbf{h}^{\mathrm{T}})$, can be estimated from the data uncertainties as described in Appendix A. The confidence region for the fitted rotation $\hat{A}$ at a selected significance level α (e.g., $\alpha = 0.05$ to produce a 95% confidence region) is defined as a collection of candidate rotations $A = \hat{A}\Phi(\mathbf{h})$ with all possible vectors **h** that satisfy the condition

$$\mathbf{h}^{\mathrm{T}}\mathrm{cov}(\mathbf{h})^{-1}\mathbf{h} \le \chi^2_\alpha[3] \tag{2}$$

where $\chi^2_\alpha[3]$ is the upper critical value of the χ^2 distribution with three degrees of freedom. Note that according to this definition, the perturbation $\Phi(\mathbf{h})$ is applied before the best-fit rotation $\hat{A}$, hence the covariance matrix is defined in the reference frame of the plate that is being reconstructed. This convention conforms with the standard practice of expressing rotation uncertainties in studies of relative plate kinematics [*Chang et al.*, 1990].

[41] The quality of fit was evaluated by comparing the observed misfit between the reconstructed track locations rotated by $\hat{A}$ and the modeled hot spot positions with the misfit expected from their uncertainties, using the statistic

$$\chi^2 = \frac{\mathrm{SSE}(\hat{A})}{\sigma^2} \tag{3}$$

where $\mathrm{SSE}(\hat{A})$ denotes the weighted sum of the squared misfits and σ^2 is the average combined variance of the data (see Appendix A for the definitions of these parameters). Assuming Fisherian-distributed errors of the data, χ^2 is distributed as $\chi^2[2n - 3]$, where n is the number of hot spots used in the reconstruction. Hence, when the χ^2 exceeded the upper critical value of the χ^2 distribution with $2n - 3$ degrees of freedom at a 5% significance level, we concluded that the fitted rotation $\hat{A}$ produced an unacceptably large misfit between the reconstructed track locations and their respective hot spots and the reconstruction should be rejected at this significance level.

3.3. Iterative Approach to the Solution

[42] The numerical method used to model the global mantle flow requires surface plate velocities prescribed as the upper boundary condition for the mantle domain (section 2.3). Hence, the calculated plume and hot spot motions depend on the absolute plate kinematics, which is not known *a priori.* Yet, the hot spot motions are essential for defining the absolute plate motions in a moving hot spot reference frame. To solve this "chicken and the egg" problem, we adopted an iterative approach [cf. *Steinberger et al.*, 2004], starting with a trial APM model to calculate plume motions, generating a new APM model by fitting hot spot tracks as described in section 3.2, and then repeating the entire process until convergence was reached and the modeled plume motions were fully consistent with the rotation parameters of the final iteration (Figure 1). Four iterations (including the initial model) were sufficient to reach the convergence with sufficient accuracy in all our models (section 4).

[43] As a starting point, we used a recent plate polygon model of *Torsvik et al.* [2010a], which incorporates the absolute plate motions of *O'Neill et al.* [2005], *Torsvik et al.* [2008], and *Steinberger and Torsvik* [2008] for the plates of Indo-Atlantic hemisphere, and of *Steinberger and Gaina* [2007] and *Duncan and Clague* [1985] for the plates in the Pacific. This model provides plate outlines (as closed polygons), stage poles and angular rotation rates at 10 Ma increments. As an approximation, we considered the plate velocity at any specific latitude and longitude to be constant during the 10 Ma intervals and equal to the average velocity defined by the stage rotation parameters. After each successive iteration, plate polygons were modified using the BPLATES routine of *Torsvik et al.* [2010a] to ensure the consistency between the positions of plate boundaries and newly defined absolute plate rotations. This procedure computes boundaries according to new absolute rotations for the Pacific and African plates and relative plate rotations within the Pacific and Indo-Atlantic hemispheres separately; the two sets of plate boundaries are then connected to produce a single, global set of plate polygons (see the Supplementary data of *Torsvik et al.* [2010a] for further details).

[44] Unlike the study of *Torsvik et al.* [2010a], who used two separate reference frames based on the Pacific and Indo-Atlantic hot spots to define absolute plate motions, the kinematic solutions produced in successive iterations of our models were obtained by fitting all hot spot tracks simultaneously and expressed as absolute rotations of the African plate (section 3.2). The absolute rotations for the Pacific plate were calculated back to chron C34y time (83.5 Ma) using plate circuit reconstructions, with the alternative chains of relative plate motion described in section 2.2. For earlier reconstructions ages, the Pacific plate could not be linked to the plates of Indo-Atlantic hemisphere through a plate circuit. However, our numerical models of plume conduit advection did not use the flow fields calculated for ages prior to 70 Ma (section 2.3); hence, the modeled plume motions did not depend on plate reconstructions for the earlier times.

4. Results

4.1. Revised Rotations

[45] Finite reconstruction rotations for the motion of the African plate relative to moving hot spots are presented in Table 2 and auxiliary material Table S2. The three sets of kinematic parameters correspond to the choices of plate circuit model that were used to reconstruct the Pacific plate (section 2.2), i.e., through the Antarctic connection and through the Australia-Lord Howe Rise plate circuit, with two alternative models for the early opening between Australia and East Antarctica [*Tikku and Cande*, 2000; Whittaker et al., submitted manuscript, 2011]. Each model of Africa motion in Table 2 and auxiliary material Table S2 went through five iterative steps to ensure the consistency between the modeled hot spot motions (section 2.3) and absolute plate kinematics, as described in section 3.3. The changes in hot spot motion between the successive iterations are illustrated in Figure 3. For the first iteration, hot spot traces were calculated using a model of the global mantle flow field, which is consistent with the absolute plate kinematics of *Torsvik et al.* [2010a].

Table 2. Finite Rotations of the African Plate Relative to Moving Hot Spots (Preferred Model)[a]

Age (Ma)	λ_{EP} (°N)	ϕ_{EP} (°E)	ρ (°ccw)	cov_{11}	cov_{12}	cov_{13}	cov_{22}	cov_{23}	cov_{33}
10.0	−36.66	146.72	1.61	0.1677E-03	0.6129E-04	−0.4133E-04	0.1170E-03	−0.2136E-04	0.1015E-03
20.0	−35.58	156.74	3.52	0.1883E-03	0.7021E-04	−0.4360E-04	0.1356E-03	−0.2297E-04	0.1139E-03
30.0	−36.19	153.99	5.85	0.2119E-03	0.8176E-04	−0.4411E-04	0.1583E-03	−0.2351E-04	0.1259E-03
40.0	−37.63	147.30	9.09	0.2352E-03	0.9647E-04	−0.4209E-04	0.1874E-03	−0.2268E-04	0.1383E-03
50.0	−42.80	147.61	9.83	0.2790E-03	0.1087E-03	−0.4877E-04	0.2186E-03	−0.2379E-04	0.1709E-03
60.0	−56.84	149.31	11.47	0.3002E-03	0.1197E-03	−0.5614E-04	0.2551E-03	−0.2999E-04	0.1974E-03
70.0	−51.40	149.04	15.75	0.4874E-03	0.1308E-03	−0.9232E-04	0.2937E-03	−0.1568E-04	0.3394E-03
80.0	−30.59	156.20	19.06	0.6708E-03	0.9605E-04	−0.8016E-04	0.3097E-03	−0.6070E-04	0.3041E-03
100.0	−16.58	156.03	24.22	0.1333E-02	−0.1991E-03	0.3362E-04	0.5669E-03	−0.1122E-03	0.6118E-03
124.0	−17.74	155.75	28.77	0.1715E-02	−0.2167E-03	0.9565E-04	0.6859E-03	−0.1429E-03	0.7294E-03

[a]Parameters are as follows: λ_{EP} and ϕ_{EP} are the latitude and longitude of the Euler pole, ρ is the rotation angle, cov_{ij} is the i-row, j-column element of the covariance matrix expressed in radians squared (i, j = 1,2,3). Because the covariance matrix is symmetric, only the upper triangle is tabulated. The covariance matrices are expressed in the reference frame of the African plate. In this model, the Pacific plate was reconstructed using Australia-Lord Howe Rise plate circuit model 1, with the Australia-Antarctica rotations of *Tikku and Cande* [2000]. Alternative kinematic solutions using the reconstructions of the Pacific plate through the Antarctic plate circuit and model 2 of the Australian plate circuit are presented in auxiliary material Table S2.

After defining a new APM model by fitting the hot spot tracks, calculating the mantle flow with the new absolute plate kinematics imposed as a boundary condition, and re-advecting plume conduits in the newly generated flow field, we observed significant changes in calculated traces for all five hot spots used in the reconstruction (compare iterations 1 and 2 in Figure 3). In subsequent iterations, the changes were notably smaller; iterations 3–5 produced indistinguishable surface plume traces. The final model (for each of three choices of the Pacific plate circuit) is based on the hot spot motions calculated after the fifth iteration.

[46] The changes of absolute kinematics with the successive iterations of the models are illustrated in Figures 4a–4c, where we plotted flowlines for an arbitrarily chosen position on the African plate, presently located at 15°N, 20°E. Similarly to the estimated surface traces of plume conduits, the most significant changes were observed between the first (red flowlines) and second iterations (magenta flowlines). Starting from the third iteration, the absolute rotations virtually did not change, and we conclude that the convergence has been reached by the fourth iteration in all models. The final iterations of the three alternative models (black flowlines) show similar changes in direction and rate of absolute plate motion for the last 124 Ma. Notably, the use of Australian plate circuits 1 and 2 (Figure 4d) produced nearly identical kinematic solutions; the differences between these two models are well below the uncertainties of estimated rotations (section 3.2). This result shows that the APM models incorporating the reconstructions of the Pacific plate through Australia and the Lord Howe Rise are not sensitive to the choice of the alternative kinematic model for the early opening between East Antarctica and Australia discussed in section 2.2.

4.2. Quality of Fit

[47] The overall quality of fit in each of the three alternative models presented in Table 2 and auxiliary material Table S2 can be visually evaluated by comparing model hot spot tracks, which were calculated using absolute plate motions and associated hot spot motions, with the geometries and age progressions along the actual tracks. Figure 5 shows the predictions for the Hawaiian and Tristan tracks obtained using the two end-member kinematic models corresponding to the worst and the best overall fit, respectively. The first model (Figures 5a and 5c) uses the Antarctic plate circuit for reconstructions of the Pacific plate (auxiliary material Table S2); the second model (Figures 5b and 5d) is based on reconstructions through the Australian plate circuit 1 (Table 2). Similar plots for all remaining hot spot tracks modeled using the alternative kinematic solutions are presented in the auxiliary material (Figures S1–S3).

[48] As seen from Figures 5b, 5d and auxiliary material Figures S2–S3, both models based on Australia-Lord Howe Rise plate circuit produced close fits to all five hot spot tracks used in the reconstruction. The model incorporating the East Antarctica-Australia rotations of *Tikku and Cande* [2000] (model 1) produced slightly smaller misfits than the model using the rotations of Whittaker et al. (submitted manuscript, 2011) (model 2). In contrast, the kinematic solution using the plate circuit through Antarctica resulted in significantly larger misfits for the Paleocene to Late Cretaceous (60–80 Ma) segments of the tracks, which are clearly identifiable in the examples shown in Figures 5a and 5c. For the Hawaiian track (Figure 5a), the model predicts a more northeastward orientation of the ~50–80 Ma segment of the track, which contrasts with a nearly northward trend of the Emperor chain, producing ~330 to 1000 km misfits for Suiko (61 Ma) and Detroit (76–81 Ma) seamounts, respectively. Similarly, a pronounced kink of the modeled Tristan track at 80 Ma (Figure 5c) and an ~800 km associated misfit clearly contrast with a gentle curvature of the Walvis Ridge. These observations suggest that the model using the Antarctic plate circuit for reconstructions of the Pacific plate did not produce an acceptable fit for the hot spot tracks in Paleocene and Late Cretaceous time, and the formal statistical test for the goodness of fit (section 3.2) confirms this suggestion.

[49] The goodness of fit statistics (χ^2, equation (A23), divided by the number of degrees of freedom for the ease of comparison) and other relevant parameters are presented in Table 3 and illustrated in Figure 6a. These values show that the model using the Antarctic plate circuit reconstructions of the Pacific plate produced formally acceptable fits for the 10–60 Ma, 100 Ma and 124 Ma rotations. However, the 70 and 80 Ma rotations produced misfits that are significantly greater than those expected from the uncertainties assigned to the data (section 3.1), even at the 1% significance level. Hence, we can conclude that the absolute kinematic model incorporating the Antarctic plate circuit is not acceptable for Late Cretaceous time. In contrast, the misfits produced by the kinematic model, in which the Pacific plate

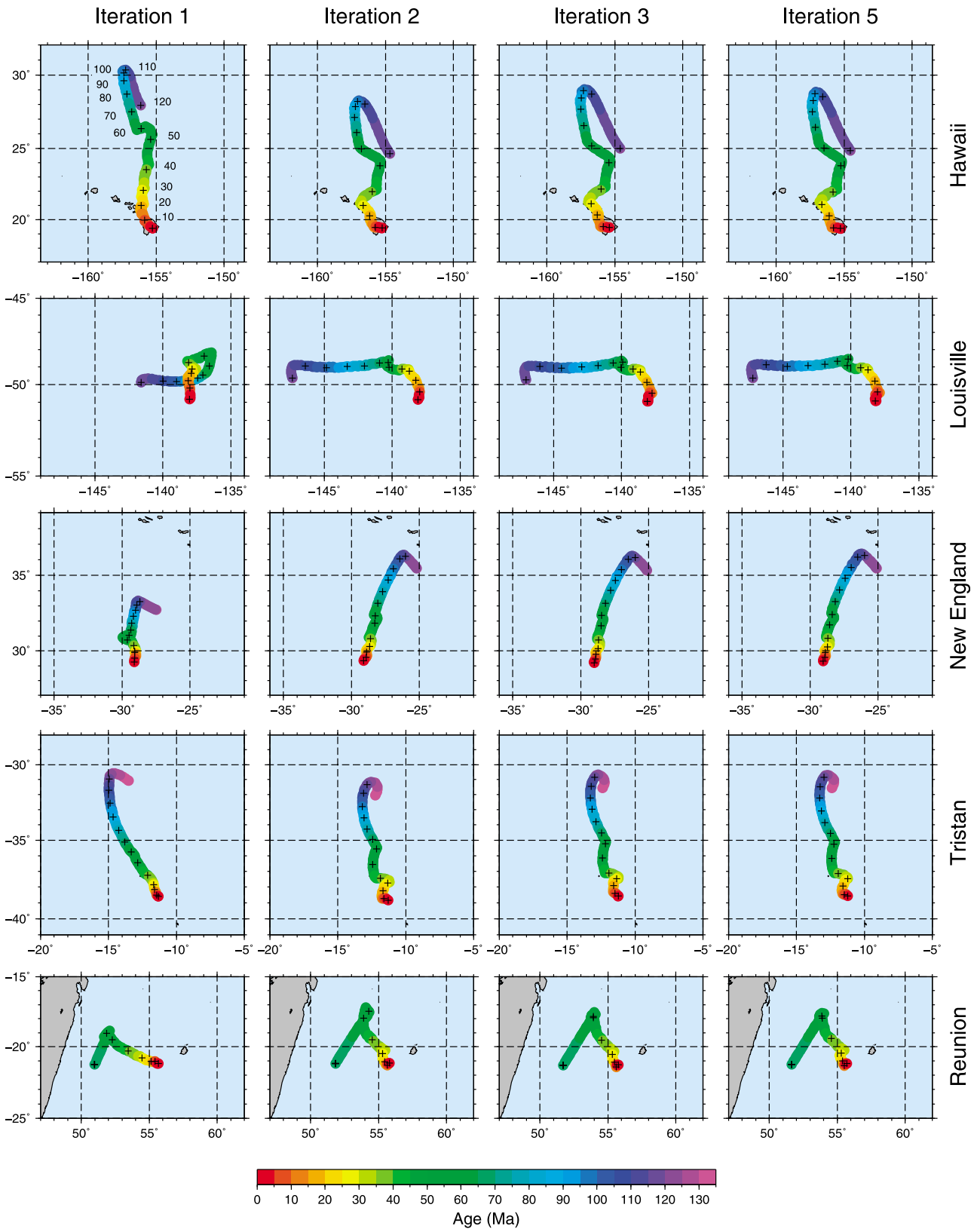

Figure 3. Modeled hot spot motions used in successive iterations of the absolute kinematic model, in which the Pacific plate was reconstructed using model 1 of the Australian plate circuit. Surface traces of hot spots are shown as rainbow-colored swaths, color-coded according to the age. Black crosses are shown at 10 Ma increments.

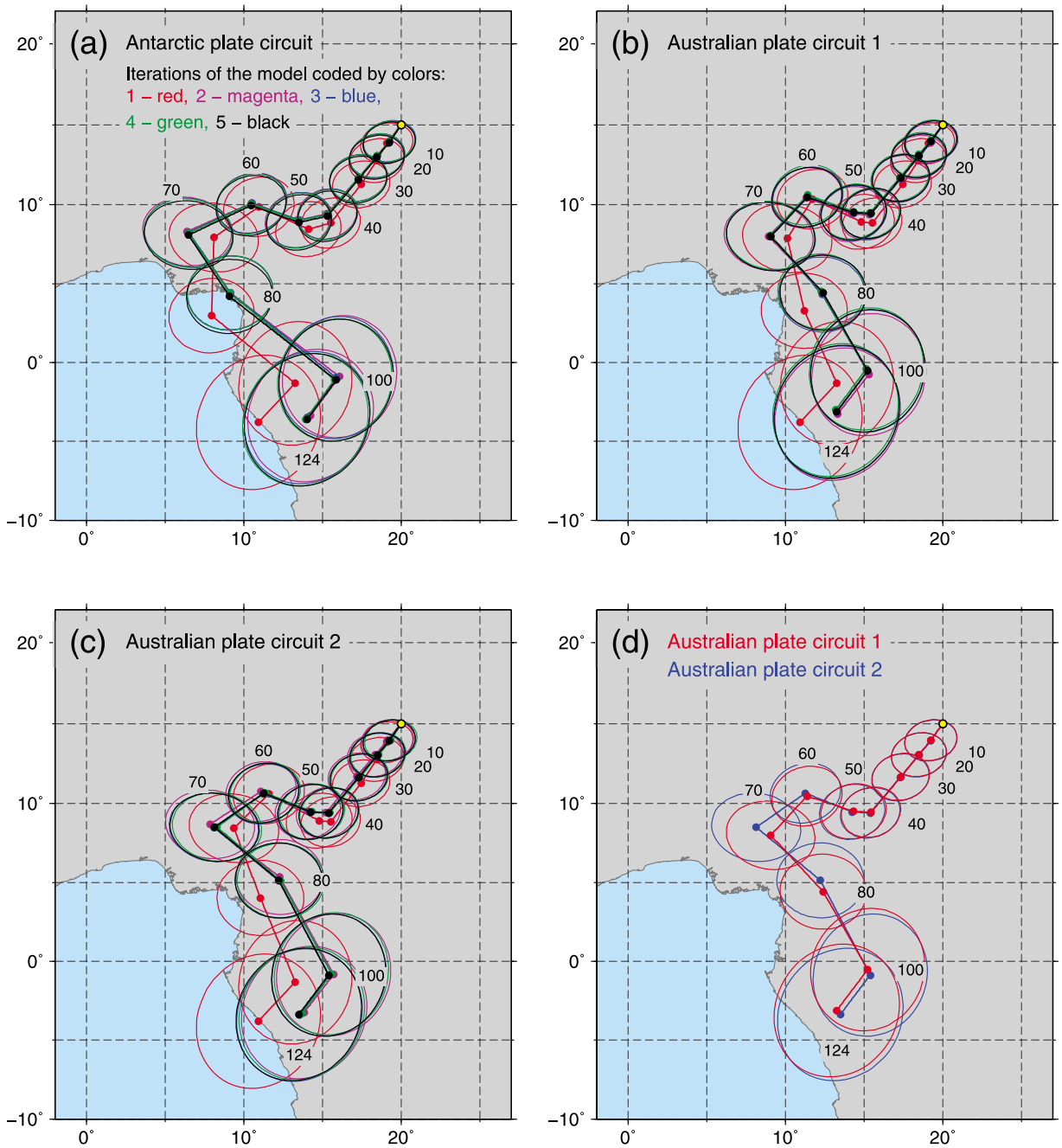

Figure 4. (a–c) Changes of absolute motion of Africa in successive iterations of alternative moving hot spot models. Motion is illustrated by reconstructing the position at 15°N, 20°E back in time. Colors denote the iterative steps. Ellipses are the 95% confidence regions for the reconstructed position. (d) A comparison of the two final models (iteration 5) that use different reconstructions of Australia-Antarctica motion in the Australian plate circuit (see text).

was reconstructed using model 1 of the Australian plate circuit, are notably smaller for early Eocene through Late Cretaceous time (50–80 Ma) and are within the limits imposed by the data uncertainties for all reconstruction ages. Similar to the model that uses the Antarctic plate circuit, the largest misfits (a RMS misfit of ~250 km, Figure 6b) were observed for the 70 and 80 Ma reconstructions. However, even for these relatively poor fits, the test values did not exceed the upper 5% critical point of the relevant χ^2 distribution (Table 3, Figure 6a), and we conclude that this model is acceptable within the entire age interval, back to 124 Ma.

[50] Almost identical results were obtained for the model incorporating the Pacific plate reconstructions through Australian plate circuit 2. Marginally acceptable fits were observed for the 70 and 80 Ma reconstructions, with the test values only slightly above the 5% critical values of χ^2 and the corresponding RMS misfits of ~280 km (Table 3). (Here we define the region of marginal consistency as the values that

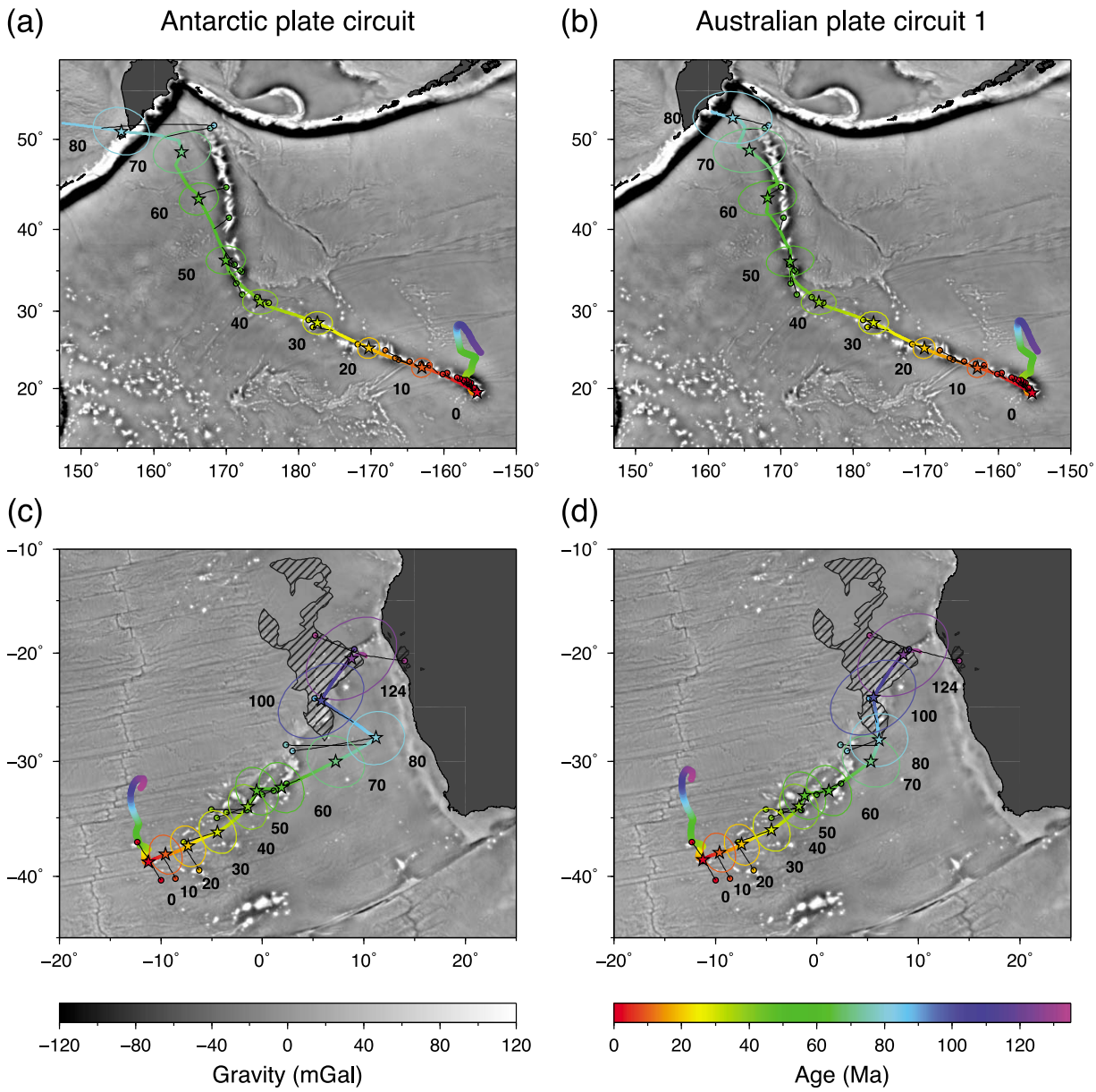

Figure 5. (a–d) Examples of fits in moving hot spot models. Model tracks of the Hawaiian and Tristan hot spots calculated by combining absolute plate motions and hot spot motions are shown as rainbow-colored paths (color-coded according to the age) with stars plotted at 10 Ma increments. Ellipses show the 95% uncertainty regions. For the Tristan track, these were calculated using the uncertainties of the African absolute motion (Table 2 and auxiliary material Table S2); for the Hawaiian track, the uncertainties of absolute rotations were propagated through the plate circuit and combined with the errors of relative plate motions using the procedure of *Doubrovine and Tarduno* [2008a]. Thicker rainbow-colored swaths, with a similar age-coloring scheme, represent the surface motions of hot spots estimated from numerical models of plume conduit advection. Small dots with tie-lines to the model hot spot tracks are the locations of radiometrically dated samples. Marine gravity anomaly maps are according to *Sandwell and Smith* [1997]. The hatched areas in Figures 5c and 5d show the Parana-Etendeka flood basalt province at 132 Ma (in south African coordinates). Figures 5a and 5c show the predictions of the model using the Antarctic plate circuit for reconstructing the Pacific plate; Figures 5b and 5d show the results based on reconstructions using model 1 of the Australian plate circuit (see text).

exceed the 5% critical point of χ^2 distribution, but do not exceed the critical value at a 1% significance level.) For the remaining reconstruction times, the fits are fully acceptable. Allowing the possibility that the uncertainties assigned to the input data may have been underestimated (see the discussion in section 3.1), we cannot reject the Late Cretaceous (70 and 80 Ma) rotations of this model, even though they have failed the formal test. Yet, we prefer the kinematic solution based

Table 3. Goodness of Fit Statistics for the Alternative Moving Hot Spot Models[a]

Age (Ma)	n	df	SSE($\hat{A}$)	RMS (km)	χ^2/df	$\chi^2_{0.05}$[df]/df
Using the Plate Circuit Through Antarctica						
10	4	5	0.1674E-02	128.1	1.237	2.214
20	4	5	0.2076E-02	139.0	1.342	2.214
30	4	5	0.1329E-02	113.7	0.754	2.214
40	4	5	0.1499E-02	136.1	0.750	2.214
50	4	5	0.3371E-02	181.8	1.387	2.214
60	4	5	0.5304E-02	226.7	1.916	2.214
70	3	3	0.1060E-01	380.7	5.554	2.605
80	3	3	0.3811E-01	707.7	18.130	2.605
100	2	1	0.1018E-03	45.5	0.112	3.841
124	2	1	0.7653E-05	12.5	0.007	3.841
Using Australia-Lord Howe Rise Plate Circuit Model 1						
10	4	5	0.1965E-02	139.3	1.452	2.214
20	4	5	0.2374E-02	148.9	1.534	2.214
30	4	5	0.1597E-02	124.3	0.906	2.214
40	4	5	0.1402E-02	130.7	0.702	2.214
50	4	5	0.1584E-02	124.9	0.651	2.214
60	4	5	0.1809E-02	134.8	0.653	2.214
70	3	3	0.4586E-02	251.2	2.403	2.605
80	3	3	0.4490E-02	243.2	2.136	2.605
100	2	1	0.3736E-03	87.2	0.413	3.841
124	2	1	0.1852E-03	61.4	0.168	3.841
Using Australia-Lord Howe Rise Plate Circuit Model 2						
10	4	5	0.1840E-02	133.1	1.359	2.214
20	4	5	0.2216E-02	142.6	1.432	2.214
30	4	5	0.1407E-02	114.8	0.799	2.214
40	4	5	0.1135E-02	117.0	0.568	2.214
50	4	5	0.1244E-02	110.0	0.512	2.214
60	4	5	0.2385E-02	152.8	0.862	2.214
70	3	3	0.5893E-02	282.7	3.088	2.605
80	3	3	0.6003E-02	279.9	2.855	2.605
100	2	1	0.1517E-03	55.5	0.168	3.841
124	2	1	0.3241E-04	25.7	0.029	3.841

[a]Parameters are as follows: n is the number of hot spots, df is the number of degrees of freedom ($2n - 3$), SSE($\hat{A}$) is the sum of weighted, squared errors for the best-fit rotation (equations (A4)–(A6)), RMS is the root mean square misfit between the reconstructed track positions and corresponding locations of hot spots estimated through numerical modeling, χ^2 is the goodness of fit statistics (equation (A23)), and $\chi^2_{0.05}$[df] is the upper critical point of the χ^2 distribution with df degrees of freedom, corresponding to a 5% probability.

on model 1 of the Australian plate circuit because it produces the best overall fit to the hot spot tracks used in our reconstructions. While the detailed kinematic history of the opening between Australia and Antarctica in Cretaceous time is still a subject of active research and refinements, we feel that the rotations of *Tikku and Cande* [2000] provide a reasonable approximation for the early Australia-Antarctica motion. We stress that the incorporation of kinematic parameters of Whittaker et al. (submitted manuscript, 2011) in the Australian plate circuit produces very minor changes for the absolute plate kinematics; the differences between the rotation parameters for the two "Australian" models presented in Table 2 and auxiliary material Table S2 are negligible in comparison with estimated rotation uncertainties.

5. Discussion

5.1. Fixed Hot Spot Models

[51] Using fixed hot spots as a reference frame [*Morgan*, 1971] has traditionally been (and still remains) a popular way of defining absolute plate kinematics. There are two key assumptions underlying this approach. First, hot spots distributed over the surface of the Earth are assumed to remain fixed relative to each other through geologic time, forming a single reference frame. Second, no significant motion of this reference frame is assumed relative to the Earth's "mean" mantle, i.e., in a reference frame, in which the convective flow within the mantle globally averages to no net motion; thus, it can be used as a proxy reference frame for the entire mantle. Considering that being an integral part of the large-scale mantle circulation, mantle plumes are entrained into the global flow, and hence their conduits are expected to move, bend and get distorted by the "mantle wind," neither of these two assumptions appears valid. A common escape from this paradox was to assume that mantle plumes and hot spots, even if not truly stationary, can nevertheless be considered as "approximately fixed" when the rate of their motion is compared to much faster velocities of surface plates.

[52] Some support for this idea comes from studies that analyzed the Pacific and Indo-Atlantic hot spot tracks separately. For instance, *O'Neill et al.* [2005] produced a fixed hot spot reference frame and a moving hot spot reference frame using hot spot tracks from the Indian and Atlantic oceans and performed a formal statistical test to determine whether the two frames are significantly distinct. They concluded that for the last 80 Ma the two Indo-Atlantic reference frames were indistinguishable, and that the hot spot motion was 'not discernible above the uncertainties in the data for times less than ~80 Ma' [*O'Neill et al.*, 2005, p. 24]. *Andrews et al.* [2006] fitted the Pacific rotations relative to the fixed Hawaiian and Louisville hot spots back to ~68 Ma and conducted a goodness of fit test using a statistical approach that is similar to the χ^2 test described in section 3.2. They found no significant misfits in their reconstructions and concluded that the assumption of fixity for the two Pacific hot spots for the last 68 Ma is viable. In contrast, estimates of great circle distance between the Hawaiian and Louisville hot spots through time [*Wessel and Kroenke*, 2009] suggested a significant decrease in their separation (by ~5°) during the ~80–55 Ma interval, indicating relative hot spot motion.

[53] Plate circuit reconstructions consistently show a limited value of fixed hot spot reference frames based solely on Pacific or Indo-Atlantic data: the reconstructions in Pacific fixed hot spot reference frames fail to reproduce the geometries of Indo-Atlantic hot spot tracks and, conversely, motion of the Pacific plate relative to the Indo-Atlantic hot spots does not fit the Pacific hot spot tracks [*Cande et al.*, 1995; *DiVenere and Kent*, 1999; *Raymond et al.*, 2000; *Doubrovine and Tarduno*, 2008a, 2008b]. These observations suggest that the Pacific and Indo-Atlantic hot spots do not constitute a single reference frame consistent with the assumption of globally fixed hot spots. We further tested global hot spot fixity by fitting absolute rotations and performing the formal test for the goodness of fit (section 3.2) for the five hot spot tracks that we have used in our moving hot spot reconstructions (Hawaii, Louisville, New England, Reunion and Tristan).

[54] The fitting procedure was analogous to the approach used to define the moving hot spot models described in section 4, except hot spots were assumed to remain stationary through time at their present locations as listed in Table 1. Because no advection of plume conduits was required for this exercise, we did not have to iterate the kinematic solutions

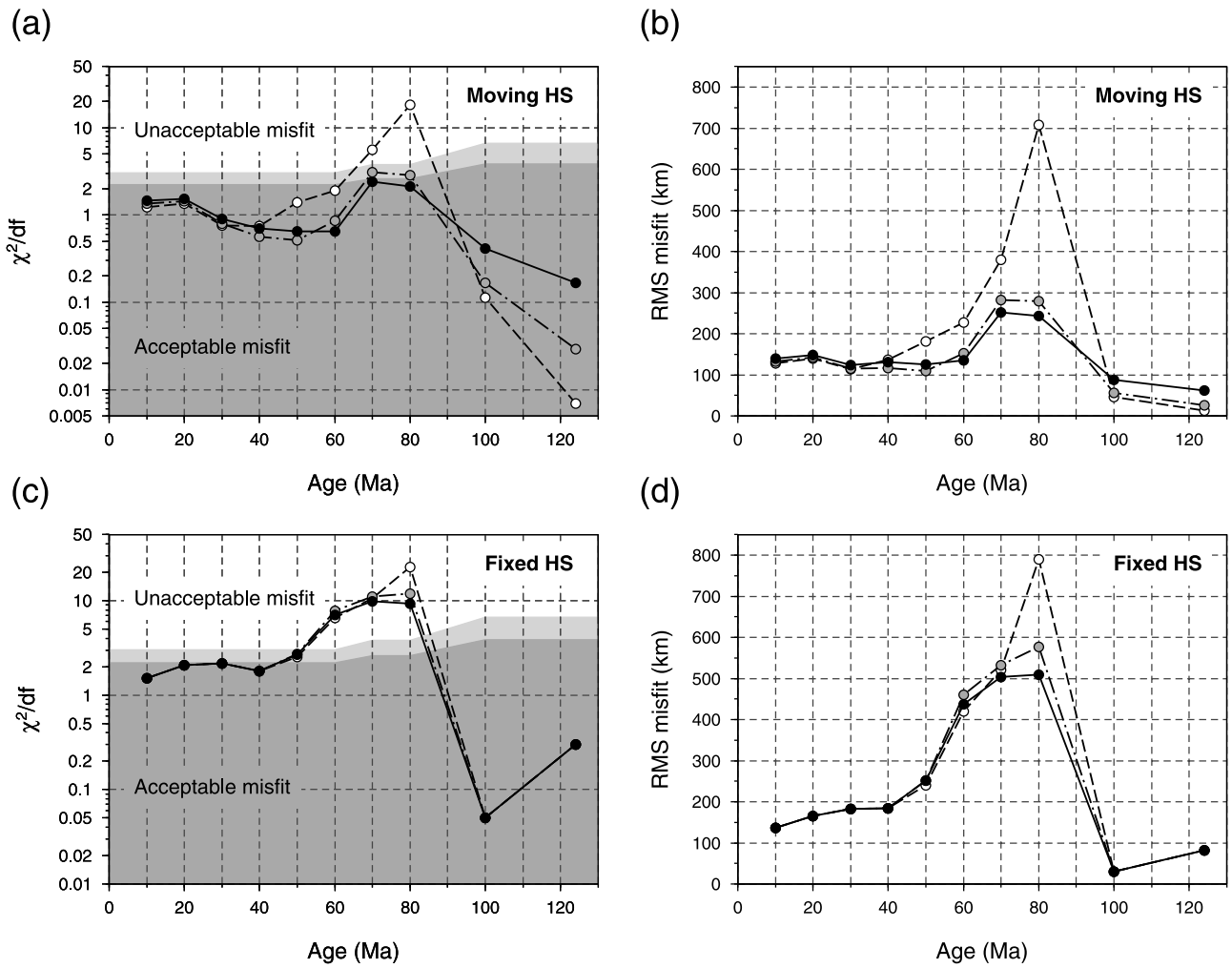

Figure 6. Goodness of fit test statistics (χ^2/df) and RMS misfits for the (a, b) alternative moving hot spot and (c, d) fixed hot spot reconstructions. Symbols denote different kinematic models used to reconstruct the Pacific plate: the Antarctic plate circuit (white circles), Australian plate circuit model 1 (black circles) and Australian plate circuit model 2 (gray circles). Darker gray field of acceptable misfit in Figures 6a and 6c correspond to the values of χ^2 that do not exceed an upper critical value of the corresponding χ^2 distribution at a 5% significance level. Lighter gray field shows the region of marginal misfit, between the critical values corresponding to the 5% and 1% significance (see text).

(cf. section 3.3) and the "final" models were obtained in one step. The errors assigned to the input data (track and hot spot locations) were kept exactly as in moving hot spot models, including the increase in the uncertainty of hot spot location with age, although the locations themselves did not change through time. The error budgets in the fixed and moving hot spot reconstructions were thus identical, so that the quality of fixed hot spot fits can be directly compared with that of moving hot spot models.

[55] The fits of the fixed hot spot models for the Hawaiian and Tristan tracks are shown in Figure 7. Similarly to Figure 5, Figures 7a and 7c show the results for the solution incorporating the Antarctic plate circuit reconstructions of the Pacific plate, while Figures 7b and 7d illustrate the fits obtained using model 1 of the Australian plate circuit. The fits produced by the fixed hot spot reconstructions for Eocene to Late Cretaceous segments of the tracks (50–80 Ma, Figure 7) are significantly worse than the corresponding fits of the moving hot spot models (Figure 5), regardless of the choice of Pacific plate circuit. This holds true for the remaining hot spot tracks (not shown in Figure 7), and is further illustrated by high RMS misfit values, that peak at ~500–800 km for the Late Cretaceous reconstructions (70 and 80 Ma, Figure 6d). Such misfits are clearly not acceptable.

[56] The results of the goodness of fit test for the fixed hot spot models are shown in Figure 6c. The high values of χ^2 statistic for the 60, 70 and 80 Ma reconstructions indicate significant misfits in all three fixed hot spot models; the probability of obtaining values as high as observed by chance does not exceed 0.001% in all cases. The fixed hot spot 50 Ma reconstructions are only marginally acceptable. Even for the 10–40 Ma rotations that produced acceptable misfits, the values of χ^2 and RMS misfit are higher than those observed in the corresponding moving hot spot models (compare Figures 6c and 6d with Figures 6a and 6b, respectively). Only the two oldest rotations (100 and 124 Ma) in the

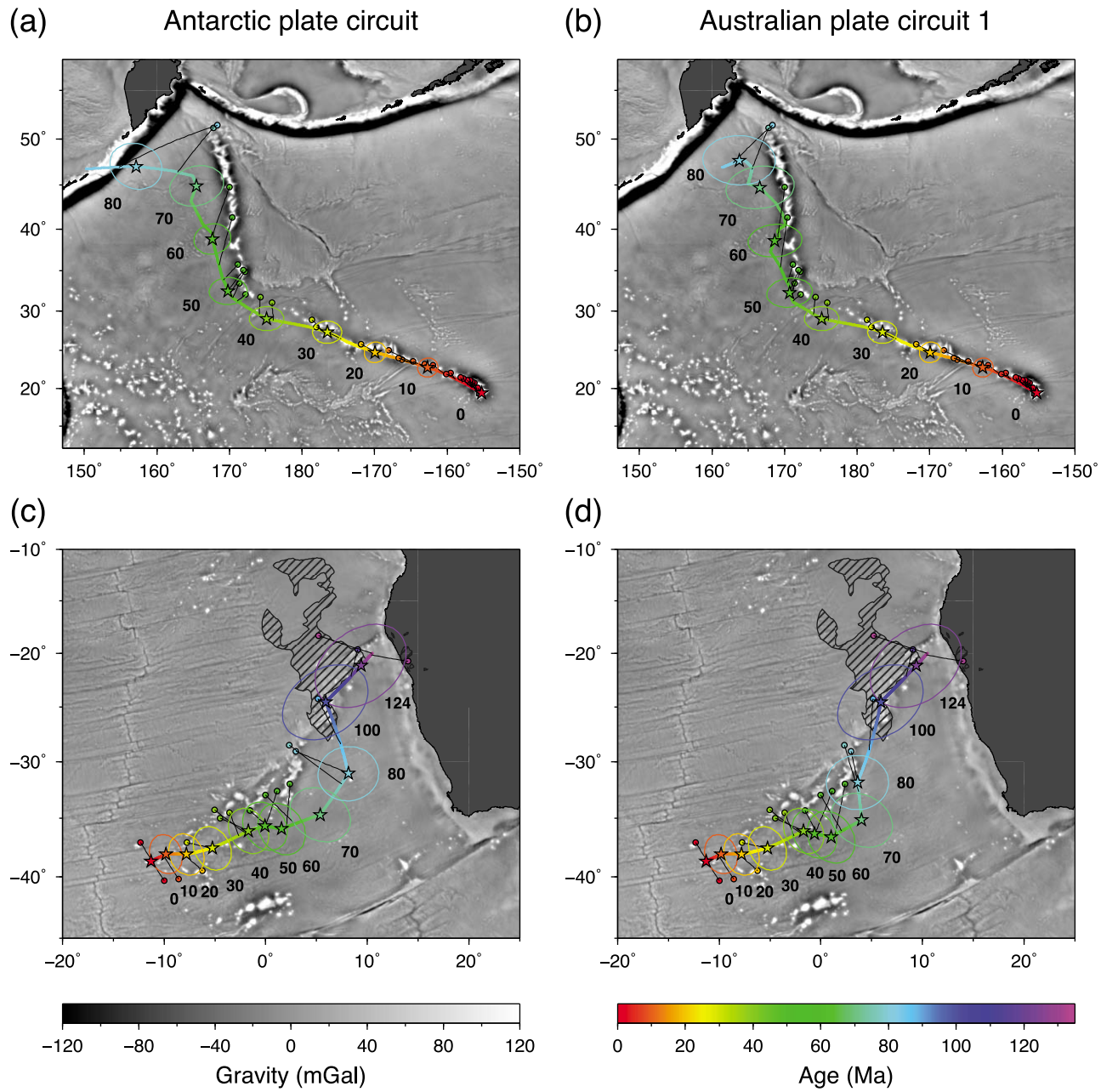

Figure 7. Examples of fits in fixed hot spot models for the Hawaiian and Tristan tracks. See the caption of Figure 5 for the description of symbols.

fixed hot spot model, which are exclusively based on the data from the Tristan and New England tracks, are of a comparable quality with the coeval rotations of the moving hot spot reconstructions.

[57] In summary, we conclude that in comparison with the moving hot spot models, the reconstructions assuming globally fixed hot spots produced inferior fits to the analyzed hot spot tracks for the entire interval from the recent to Late Cretaceous time (10–80 Ma). For the Paleocene to Late Cretaceous (60–80 Ma), the fixed hot spot models resulted in clearly unacceptable misfits, no matter what kinematic model was used for the reconstructions of the Pacific plate. This is an expected result, once again highlighting the significance of motion between the Pacific and Indo-Atlantic hot spots in Late Cretaceous and Paleocene time [cf. *Doubrovine and Tarduno*, 2008a]. Following *Torsvik et al.* [2008], we strongly suggest that fixed hot spot reference frames should no longer be used.

5.2. Comparison With Published Hot Spot Frames

[58] Hot spot reconstructions have been routinely used by the geophysical community for modeling absolute plate motions from the early Cretaceous to recent time (~120–0 Ma), and it is important to address the extent of revisions suggested by our new global moving hot spot reference frame (GMHRF) in comparison to the existing hot spot frames. When referring to the GMHRF, we will henceforth mean our preferred kinematic solution, which incorporates

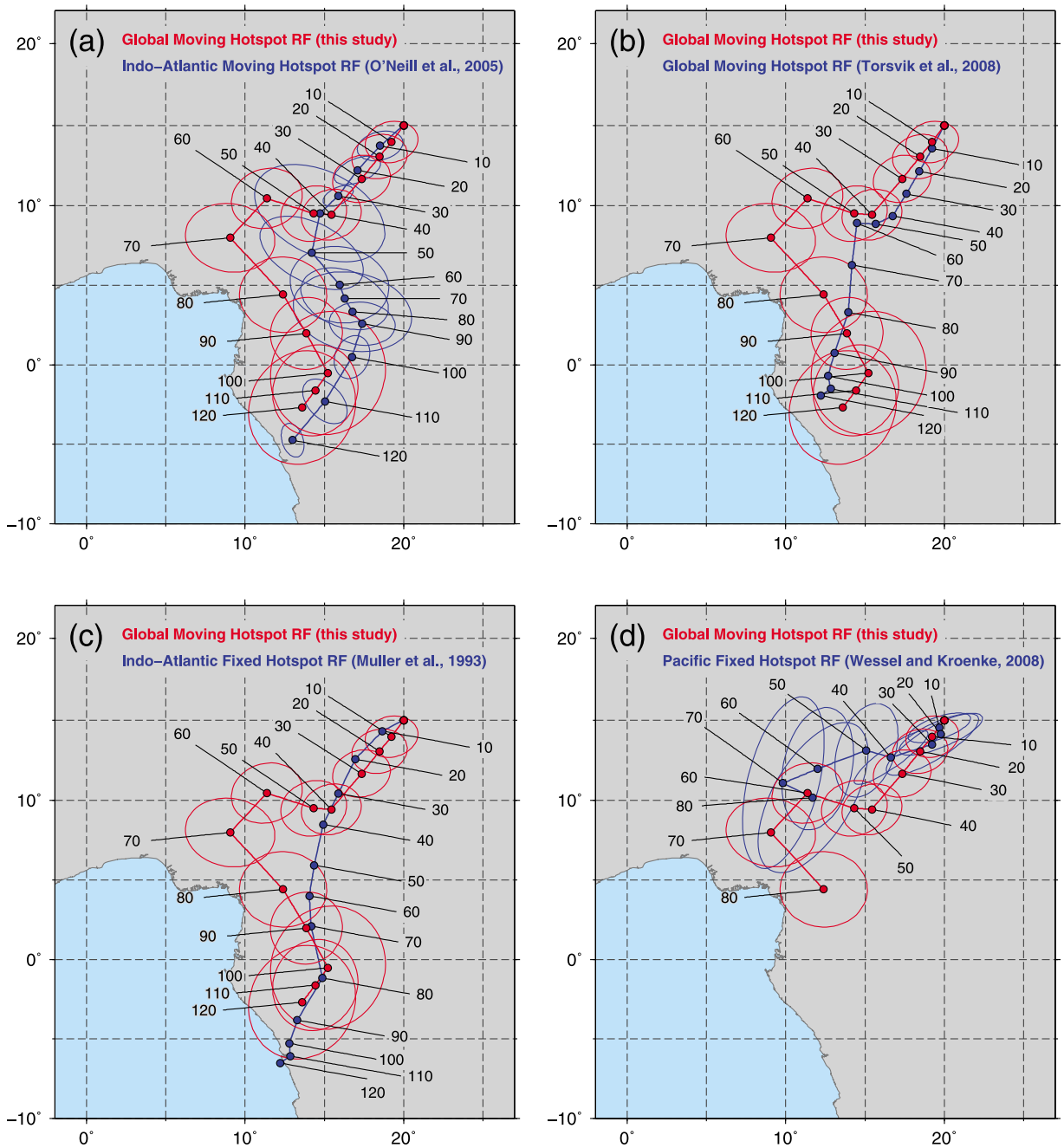

Figure 8. Estimates of the African motion in hot spot reference frames. The motion since 120 Ma is illustrated by constructing reference flowlines at 10 Ma increments, similar to those shown in Figure 4. Red flowlines (identical in all subfigures) correspond to the motion in the GMHRF. Blue lines are the estimates based on the moving hot spot frames of (a) *O'Neill et al.* [2005] and (b) *Torsvik et al.* [2008], and fixed hot spot frames of (c) *Müller et al.* [1993] and (d) *Wessel and Kroenke* [2008].

reconstructions of the Pacific plate relative to Africa using model 1 of the Australian plate circuit (Table 2). For the purpose of illustration, we considered the motion of Africa relative to moving or fixed hot spots that define the reference frames discussed below. The choice of analyzing the predictions of Africa absolute motion was made because Africa is the reference plate of the GMHRF (section 2.2), as well as virtually all earlier Indo-Atlantic and global hot spot reference frames.

[59] The motion of Africa in the GMHRF (or any other absolute reference frame) can be visualized by plots similar to Figure 4, in which we reconstructed an arbitrarily chosen location on the African plate back in time, constructing a reference flowline, which is the path traveled by the location to its present-day position at 15°N and 20°E. Figure 8 shows this flowline (the red line identical in all sub-figures, GMHRF) and similarly constructed paths in the Indo-Atlantic moving hot spot reference frame of *O'Neill et al.* [2005],

global moving hot spot frame of *Torsvik et al.* [2008], fixed Indo-Atlantic hot spot frame of *Müller et al.* [1993], and fixed Pacific hot spot frame of *Wessel and Kroenke* [2008] (blue lines). For the ease of comparison, we interpolated the rotations at 10 Ma increments (wherever they had not been estimated at 10 Ma steps originally) and estimated the uncertainties of interpolated rotations following the procedure described by *Doubrovine and Tarduno* [2008a]. Ages of the *Müller et al.* [1993] rotations were adjusted to the timescales of *Cande et al.* [1995] back to 83.5 Ma, and of *Gradstein et al.* [1994] for earlier times, to ensure the timescale consistency for all models. *Torsvik et al.* [2008] pointed out that such an adjustment is not a strictly valid way of "updating" an existing hot spot reference frame with a more recent timescale because fixed hot spot reconstructions combine relative plate motions, which are sensitive to the use of a different timescale, and radiometric dates from hot spot tracks, which are not (sections 2.1 and 2.2). The proper approach would be redoing the analysis of *Müller et al.* [1993] with the ages of relative plate rotations modified according to the timescales of *Cande et al.* [1995] and *Gradstein et al.* [1994]; this, however, is outside the scope of our study. Furthermore, *Torsvik et al.* [2008] showed that a simple age adjustment adopted here results in very minor modifications of the reference frame of *Müller et al.* [1993], with the differences between the reconstructions using the original and age-adjusted rotations less than ~100 km.

[60] Comparing the reconstructions of Africa in the GMHRF and in the Indo-Atlantic reference frame of *O'Neill et al.* [2005] (Figure 8a), we did not observe significant differences between the two models for the past 40 Ma and for the 100–120 Ma interval. However, for the times between ~50 and 90 Ma the reference flowlines depart considerably. The GMHRF predicts two prominent changes in the direction of the African motion, from a northeast to a northwest direction at 100 Ma and then back to a dominantly northeastern orientation at 70 Ma. Similar, albeit less pronounced directional changes are observed at ~90 Ma and 50 Ma in the Indo-Atlantic frame of *O'Neill et al.* [2005]. The rates of absolute motion also differ substantially. Given the reconstruction uncertainties, the differences between the two frames during the 90–50 Ma interval are significant and can be unequivocally attributed to the use of the Pacific hot spot tracks for defining the GMHRF and large-scale differential motion between the Pacific and Indo-Atlantic hot spots (sections 1 and 5.1).

[61] The consistency of the 100–120 Ma reconstructions in the GMHRF and Indo-Atlantic moving hot spot frame is not surprising, since for that time interval the GMHRF is based on Indo-Atlantic tracks only. The similarity of the two reference frames for the last 40 Ma was also expected. Our models of plume conduit advection predict ~300 km of total surface motion for the Hawaiian hot spot since 40 Ma, and less than 200 km for all remaining hot spots (Figure 3). Recalling that even the fixed hot spot model produced acceptable reconstructions for this time interval (section 5.1), the consistency of the two reference frames over the last 40 Ma can be explained by minor amounts of hot spot motion that did not produce significant systematic discrepancies between the Pacific and Indo-Atlantic hot spot groups.

[62] The reference frame of *Torsvik et al.* [2008] is an update of the earlier analysis by *Steinberger et al.* [2004] and is most compatible with our new GMHRF overall. This model uses a similar selection of hot spot tracks (except excluding the data from the New England seamounts), the same modeling technique for estimating hot spot motions (section 2.3) and a similar kinematic model of relative plate motions, including the reconstructions of the Pacific plate through the Australian plate circuit. Relative plate motions used by *Torsvik et al.* [2008], however, are not entirely identical to those implemented in the GMHRF (see section 2.2 for the description of the updates); their plate polygon model, required to assign surface plate velocities for the calculation of global mantle flow field, also differs from this study. Consequently, and because geodynamic model parameters are somewhat different here, the hot spot motions estimated by *Steinberger et al.* [2004] and *Torsvik et al.* [2008] differ from those used to define the GMHRF (compare Figure 3 and *Steinberger et al.* [2004, Figure S1]). Notably, while the amount of southward drift of the Hawaiian hot spot since Late Cretaceous time (~8° from 80 Ma to recent, Figure 3) is similar to that estimated by *Steinberger et al.* [2004], our calculations indicate smaller displacements to the east and a more complex geometry of the surface plume trace. Our model also predicts larger amounts of eastward motion for the Louisville hot spot and slightly longer surface traces for the Tristan and Reunion plumes. Whereas in the models of *Steinberger et al.* [2004] and *Torsvik et al.* [2008] the overall hot spot motion is dominated by the south–southwest drift of the Hawaiian hot spot, it is partitioned more evenly between the five hot spots used to define the GMHRF. Another important difference is the fitting approach used by *Torsvik et al.* [2008] to estimate the absolute rotations for the African plate (see *Steinberger* [2000] for details), in which three stage rotations (0–43.8 Ma, 43.8–61.2 Ma and 61.2–83.5 Ma) were calculated using a least squares regression technique (with no estimates of the rotation uncertainty) and then combined to produce a final set of finite rotations. Although the reference frame of *Torsvik et al.* [2008] extends to ~130 Ma, only reconstructions back to 83.5 Ma are based on the global fit of hot spot tracks; the rotations corresponding to the older reconstruction ages were estimated by adding stage rotations of the fixed Indo-Atlantic hot spot frame of *Müller et al.* [1993].

[63] Despite the differences discussed above, the comparison of the *Torsvik et al.* [2008] reference frame and the GMHRF (Figure 8b) shows that they are broadly consistent for the reconstruction times from 0 to 50 Ma and for the 80–120 Ma interval. For these reconstruction ages, the positions along the reference flowline for the *Torsvik et al.* [2008] model fall within the 95% uncertainty regions of those reconstructed in the GMHRF, which indicates that the two sets of rotations are not statistically distinct at the 5% significance level. Only the 60 and 70 Ma rotations appear to be significantly different. The departure originates from the differences in estimated hot spot motions, and can also be in part due to the differences in regression algorithms and weighting schemes for the input data used in the two models. For example, the GMHRF produces a better fit for the Emperor Seamounts of the Hawaiian hot spot track (Figure 5b) compared to the model of *Torsvik et al.* [2008] (e.g., a 200 km misfit versus ~300 km at 75 Ma), but slightly looser fit to the Late Cretaceous segment of the Walvis Ridge (Figure 5d, 70–80 Ma), which is acceptable

nevertheless. Because of the overall good fit of the GMHRF to the hot spot tracks in both the Indo-Atlantic and Pacific oceanic domains and the statistically rigorous approach used to define the absolute rotations, the GMHRF supersedes the reference frames of *O'Neill et al.* [2005], *Steinberger et al.* [2004], and *Torsvik et al.* [2008].

[64] Although fixed hot spot reference frames are not truly compatible with moving hot spot reconstructions, we feel it would be useful to provide examples on how our results compare with predictions of some popular fixed hot spots models. Specifically, we will consider the fixed Indo-Atlantic hot spot reference frame of *Müller et al.* [1993] (Figure 8c), which has been a standard and the most-cited reference for absolute plate kinematics for almost two decades, and the most recent Pacific hot spot reference frame of *Wessel and Kroenke* [2008] (WK08-A, Figure 8d). The latter provides absolute rotations for the Pacific plate back to the earliest Cretaceous time (144 Ma), but the rotations for the African plate could not be extended beyond 83.5 Ma because there is no suitable plate circuit linking the Pacific and African plates prior that time [e.g., *Larter et al.*, 2002]. The African absolute rotations in the reference frame of *Wessel and Kroenke* [2008] were calculated by adding relative plate motions to the absolute motion of the Pacific plate using our preferred model of the Australian plate circuit.

[65] The motion of the African plate in the reference frame of *Müller et al.* [1993] is generally similar to the GMHRF estimates for the last 40 Ma, although the fixed hot spot frame implies slightly higher velocities (Figure 8c). For the earlier ages, the positions reconstructed relative to the fixed Indo-Atlantic hot spots fall significantly further south, which is a sensible outcome considering that the plume advection model (Figure 3) predicts dominantly southward motion of Indo-Atlantic hot spots. This motion is ignored in the fixed hot spot reconstruction, resulting in artificially larger amounts of the northward displacement of Africa. The reference flowline for the *Müller et al.* [1993] frame shows a smoother trajectory, with only one sharp kink at 80 Ma. In contrast, the motion of Africa in the fixed Pacific hot spot reference frame (Figure 8d) closely mimics the directional changes observed in the GMHRF since 80 Ma. The *Wessel and Kroenke* [2008] model predicts slightly slower and more easterly oriented motion for the last 70 Ma; for the last 20 Ma, it produces reconstructions that are not statistically distinguishable from those relative to the global set of moving hot spots.

5.3. Plate Velocities and Net Lithosphere Rotation

[66] Surface velocity fields corresponding to the absolute plate motions in the GMHRF are shown in auxiliary material Figures S4–S8. Plate boundaries in this figure represent the plate polygon model produced in the final iteration of the GMHRF (see section 3.3). Plate velocities, averaged over 10 Ma intervals, were estimated by computing stage rotations and angular velocities for successive time intervals, using the equations

$$S_{12} = A_2 A_1^{\mathrm{T}} \tag{4}$$

$$\boldsymbol{\omega} = -\frac{\rho_s}{t_2 - t_1}\begin{pmatrix} \cos\lambda_s \cos\phi_s \\ \cos\lambda_s \sin\phi_s \\ \sin\lambda_s \end{pmatrix} \tag{5}$$

where A_1 and A_2 are the finite rotations (expressed as rotation matrices) corresponding to the reconstruction ages t_1 and t_2 ($t_2 > t_1$), respectively, S_{12} is the reconstruction stage rotation for the time interval between t_1 and t_2, λ_s and ϕ_s are the latitude and longitude of the Euler stage pole, ρ_s is the stage rotation angle, and ω is the angular velocity vector for the forward plate motion.

[67] The finite rotations, stage rotations and angular velocities for several major lithospheric plates (Africa, North America, South America, Eurasia, India, Australia, East Antarctica and Pacific) are presented in auxiliary material Tables S3–S5. The variations of the angular rotation rate through time are plotted in auxiliary material Figure S9. The uncertainties of finite and stage rotations, and covariance matrices of angular velocity vectors, were estimated using the formulations of *Doubrovine and Tarduno* [2008a]. The errors of relative plate reconstructions (wherever they were available) were propagated through plate circuits and combined with the uncertainties of African absolute motion. In cases when the uncertainties of relative motions have not been estimated in the original studies (typically, for the reconstruction ages older than 79.1 Ma or 83.5 Ma), the covariances are underestimated and include only the uncertainties of absolute motion.

[68] The absolute rotations of the Pacific plate for the reconstruction ages older than 83.5 Ma were calculated by combining stage rotations from the three alternative fixed Pacific hot spot models [*Duncan and Clague*, 1985; *Koppers et al.*, 2001; *Wessel and Kroenke*, 2008] with the 83.5 Ma rotation of the Pacific plate relative to the GMHRF; no uncertainty estimates are available for these reconstructions. This approach assumed that the Pacific hot spots have been fixed prior to 83.5 Ma, which is not likely. *Koppers et al.* [2001] found that the age progressions along the Pacific hot spot tracks were not compatible with the predictions of fixed hot spot models [e.g., *Duncan and Clague*, 1985; *Wessel and Kroenke*, 1997], including their own kinematic solution. Because the hot spot motions were neglected in these models, the Pacific plate reconstructions for the ages older than 83.5 Ma are subject to large, unquantified uncertainties, and any result based on these estimates should be considered with a good measure of skepticism. We also note that the stage rotations of *Duncan and Clague* [1985] for the times older than ~81 Ma (74 Ma in the original publication, the minimum age estimate from the Meiji seamount of the Emperor seamount chain) are based on radiometric ages, which were discredited by more recent studies [*Koppers et al.*, 1998, 2001; *Davis et al.*, 2002]. Recognizing that these pre-81 Ma stage rotations are a legacy model that should no longer be used in plate reconstructions, we included them only for the purpose of comparison with the earlier studies that incorporated the kinematic parameters of *Duncan and Clague* [1985].

[69] Using the angular velocities and the plate polygon model, a velocity vector (**v**) can be estimated for any particular location as

$$\mathbf{v} = (\boldsymbol{\omega} \times \mathbf{r}) \cdot R_E \tag{6}$$

where **r** is the unit vector corresponding to the location for which the velocity is being calculated, R_E is the Earth's radius, and the "×" sign denotes the vector product. The

Table 4. Net Rotation of Lithosphere[a]

Time (Ma)	λ_{net} (°N)	ϕ_{net} (°E)	ω_{net} (°/Ma)
1–0	−41.36	65.89	0.185
10–1	−45.84	58.18	0.192
20–10	−43.84	38.86	0.180
30–20	−42.95	57.25	0.137
40–30	−57.82	−168.89	0.113
50–40	−2.70	141.62	0.196
60–50	26.91	99.67	0.350
70–60	43.55	34.79	0.239
80–70	−36.61	19.40	0.483
Using Duncan and Clague [1985]			
90–80	−60.96	96.21	0.444
100–90	−40.59	123.34	0.458
110–100	−24.53	96.66	0.272
120–110	−23.29	86.30	0.297
Using Koppers et al. [2001]			
90–80	−59.63	68.87	0.341
100–90	−35.44	101.92	0.259
110–100	−34.16	88.26	0.180
120–110	−21.53	93.27	0.295
Using Wessel and Kroenke [2008]			
90–80	−62.15	71.37	0.359
100–90	−56.21	87.87	0.313
110–100	−39.14	93.30	0.299
120–110	−39.42	118.12	0.379

[a]Parameters are as follows: λ_{net} and ϕ_{net} are the latitude and longitude of the rotation pole, ω_{net} is the angular velocity.

absolute values of **v** are shown as color maps in auxiliary material Figures S4–S8. Because these values are highly sensitive to the angular distance to the stage pole, we also computed an average velocity for each plate using a 5° by 5° latitude-longitude grid, as

$$\bar{v}_{plate} = \frac{\sum_i v_i \cos\lambda_i}{\sum_i \cos\lambda_i} \tag{7}$$

where $v_i = |\mathbf{v}_i|$ is the velocity at the i'th grid point, λ_i is the latitude, and $\sum_i$ denotes summation over all points within the plate polygon. The average values and full ranges of observed velocities for the selected plates are shown in auxiliary material Figure S10.

[70] We further used the calculated plate velocities to estimate net lithosphere rotation. The angular velocity of net rotation ($\boldsymbol{\omega}_{net}$) was computed as the total angular momentum of all plates divided by the moment of inertia of the entire lithosphere (assuming a constant lithosphere thickness), using the equation [e.g., *Torsvik et al.*, 2010a],

$$\boldsymbol{\omega}_{net} = \frac{3}{8\pi R_E}\int_{-\pi}^{\pi}\int_{0}^{2\pi}(\mathbf{r}\times\mathbf{v})\cos\lambda d\lambda d\phi \tag{8}$$

The $\boldsymbol{\omega}_{net}$ values for the 10 Ma time intervals are presented in Table 4 and illustrated in Figure 9.

[71] For the most recent interval (10–0 Ma), our estimate of 0.19°/Ma net rotation is slightly higher than those of *Torsvik et al.* [2008, 2010a] (0.165°/Ma and 0.14°/Ma, respectively) and is below the 0.26°/Ma upper limit suggested by *Conrad and Behn* [2010] from the analysis of global mantle flow models and seismic anisotropy. For the past 50 Ma, net lithosphere rotation in the GMHRF is generally slow, averaging to 0.17 ± 0.03°/Ma (mean and standard deviation quoted), which is higher than the average net rotation rate estimated by *Torsvik et al.* [2010a] for this time interval (0.12 ± 0.03°/Ma). Similar to the results of *Torsvik et al.* [2010a], our model predicts a significant component of westward lithosphere drift during the past 30 Ma, and we observed a systematic increase of the net rotation rate during the last 40 Ma.

[72] The higher rates of net lithosphere rotation during the 70–50 Ma interval, especially the 60–50 Ma spike observed in the model of *Torsvik et al.* [2010a] (0.33°/Ma, Figure 9) and other reference frames, has been attributed to the fast motion of the Indian plate (e.g., auxiliary material Figures S5, S9–S10). A similar 60–50 Ma spike was observed in the GMHRF (0.35°/Ma). Noting that the poles for the 70–60 Ma and 60–50 Ma net rotations (Table 4) are close to the reconstructed position of the Indian plate (auxiliary material Figure S5), we suggest that the overall northward motion of large oceanic plates in the Pacific domain (the Pacific, Farallon and Kula plates), which moved slower than the Indian plate but comprised a much greater percentage of the lithosphere, is a more likely explanation for the high rates of net rotation during the 70–50 Ma interval.

[73] The net rotation predicted by the GMHRF during the 80–70 Ma period (0.48°/Ma) is unrealistically fast compared to the results of geodynamic models [*Becker*, 2006; *Conrad and Behn*, 2010]. The estimates for the earlier reconstruction times (120–80 Ma) depend on the choices of the fixed hot spot models used for the reconstructions of the Pacific plate prior to 83.5 Ma, with the net rotation rates varying between 0.18°/Ma and 0.34°/Ma for the model that incorporates the rotations of *Koppers et al.* [2001], 0.30°/Ma and 0.38°/Ma for the model based on reconstructions of *Wessel*

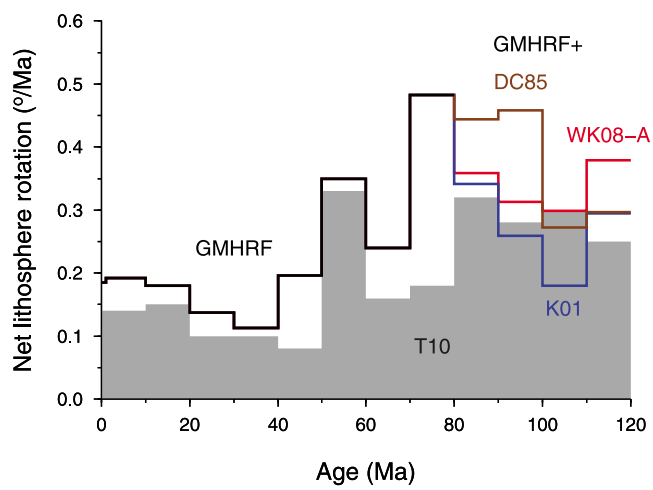

Figure 9. Net lithosphere rotation in the GMHRF (black line) compared to the estimates of *Torsvik et al.* [2010a] (shaded gray bars labeled "T10"). For the 80–120 Ma interval, estimates from three alternative models are shown (auxiliary material Figures S6–S8). The "DC85" (brown line) denotes the model in which the Pacific plate was reconstructed using the rotations of *Duncan and Clague* [1985], the "K01" (blue line) refers to the model incorporating the rotations of *Koppers et al.* [2001], and the "WK08-A" (red line) corresponds to the model based on reconstructions of *Wessel and Kroenke* [2008].

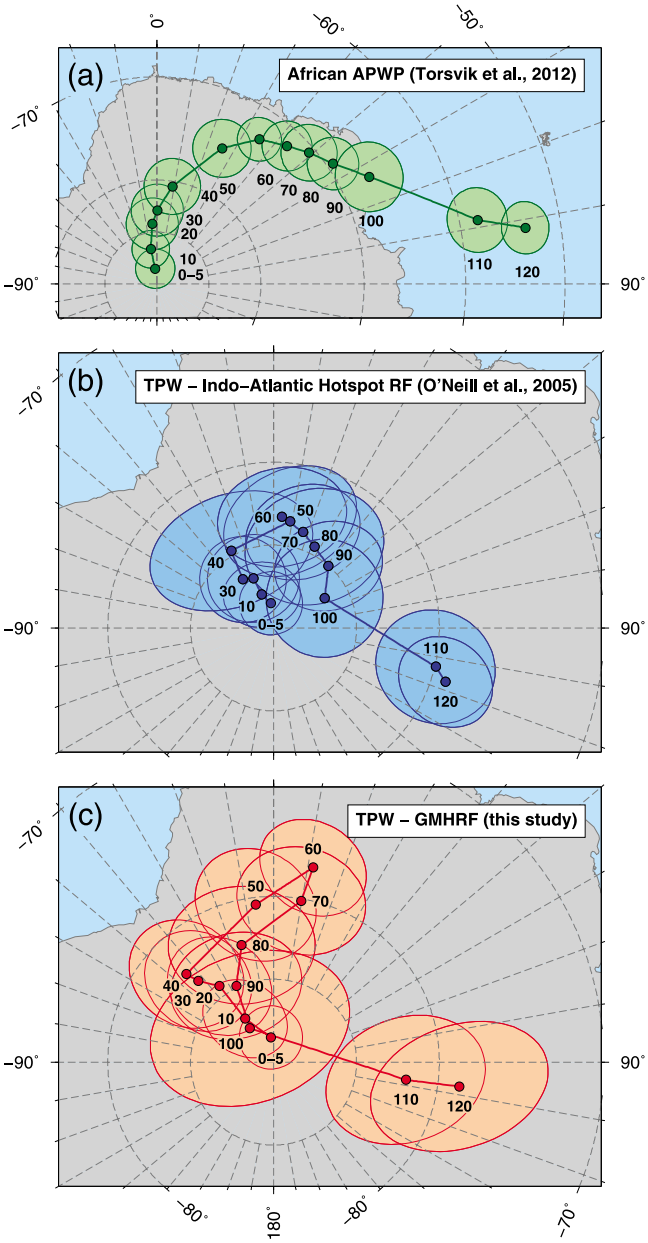

Figure 10. (a) Synthetic apparent polar wander path of *Torsvik et al.* [2012] in south African coordinates (the south poles shown) and estimates of true polar wander obtained by transferring the poles into the Indo-Atlantic moving hot spot frame of (b) *O'Neill et al.* [2005] and (c) GMHRF. The mean poles and their 95% confidence circles (A_{95}) in Figure 10a were estimated by averaging individual paleomagnetic poles rotated to Africa using a 20 Ma sliding window at 10 Ma steps. The ellipses in Figures 10b and 10c show the 95% confidence regions for transferred poles that combine intrinsic pole uncertainties and uncertainties of absolute plate rotations [*Doubrovine and Tarduno*, 2008a].

and Kroenke [2008], and 0.27°/Ma and 0.46°/Ma for the model that uses the rotations of *Duncan and Clague* [1985].

[74] We do not consider the estimates of net lithosphere rotation for the ages older than 70 Ma reliable, because for these reconstruction ages, the plate polygons representing the oceanic areas are overly simplified. For example, reconstructions of the Ontong Java, Manihiki and Hikurangi plateaus in the western Pacific Ocean [*Taylor*, 2006; *Chandler et al.*, 2012] suggested that two additional oceanic plates were spreading from the Pacific, Farallon and Phoenix plates in this region during the 123–86 Ma interval; these plates were not included in our analysis. Furthermore, it is likely that more plate boundaries (and hence more plates whose motions are uncertain) have existed due to intraoceanic subduction and concomitant back-arc spreading in the paleo-Pacific ocean of Cretaceous time. Possible fragmentation of subducting oceanic plates at active continental margins adds an extra degree of complexity to this problem. Despite some attempts to constrain the positions of intra-Pacific subduction zones using the remnants of subducted slabs imaged in the mantle by seismic tomography [*van der Meer et al.*, 2010], our knowledge of the Cretaceous plate configurations in the Pacific basin is still very much rudimentary. For the purpose of this study, we used a simple model, in which four large oceanic plates (Farallon, Izanagi, Pacific and Phoenix) encompass the entire ocean. Motions of these vast oceanic plates (especially Izanagi, Farallon and Phoenix, auxiliary material Figure S5–S8) make a dominant contribution to the estimates of net lithosphere rotation for Cretaceous time. Because this model does not capture the full complexity of plate distribution within the Pacific basin, the net lithosphere rotations for ages older than 70 Ma are likely to be overestimated.

5.4. Implications for True Polar Wander

[75] True Polar Wander (TPW) is a rotation of the entire solid Earth with respect to the spin axis that occurs in response to the gradual redistribution of density heterogeneities in the mantle and corresponding changes of the planetary moment of inertia [e.g., *Goldreich and Toomre*, 1969]. A traditional approach for estimating TPW is to compare global paleomagnetic data referenced to a single lithospheric plate with the motion of that plate in an absolute reference frame corresponding to the Earth's mantle [*Morgan*, 1981; *Besse and Courtillot*, 2002; *Torsvik et al.*, 2008]. All available high-quality paleomagnetic poles are reconstructed relative to a select plate (e.g., Africa) and then averaged (using a sliding age window or spherical splines) to produce a smoothed synthetic apparent polar wander path (APWP). Assuming that the time-averaged geomagnetic field has the geometry of a geocentric dipole aligned parallel to the Earth's spin axis, or at least that possible persistent non-dipole contributions have been negligibly small compared to the main dipole component throughout the geologic history [e.g., *McElhinny et al.*, 1996; *Tarduno et al.*, 2002; *Courtillot and Besse*, 2004; *McElhinny*, 2004], the APWP reflects the motion of the plate relative to the spin axis. Two principal components contribute in the observed APWP: (i) absolute plate motion relative to the mantle, and (ii) possible rotation of the solid Earth (mantle and lithosphere) with respect to its spin axis (TPW). By subtracting the absolute plate motion from that corresponding to the motion relative to the spin axis, it is thus possible to determine the variation in the spin axis position through time in the mantle reference frame, which provides us an estimate for the rate and direction of TPW.

[76] Figure 10 shows the synthetic APWP for the African plate (south pole positions plotted) from the most recent compilation of global paleomagnetic data by *Torsvik et al.* [2012] and the estimated TPW paths based on the use of the Indo-Atlantic moving hot spot reference frame of *O'Neill et al.* [2005] and the GMHRF. The compilation of *Torsvik et al.* [2012] is a major update of the global paleomagnetic database that corresponds to a nearly two-fold increase in the number of poles used to define the synthetic APWP compared to the earlier works [*Torsvik et al.*, 2001; *Besse and Courtillot*, 2002; *Torsvik et al.*, 2008], includes inclination shallowing corrections for the data derived from clastic sedimentary rocks, refined relative plate reconstructions that are fully consistent with those used in our study for the last ~130 Ma, and provides improved temporal coverage and spatial resolution of the APWP (Figure 10a). The synthetic poles for the last 120 Ma were transferred to the moving hot spot reference frames by reconstructing their positions (together with Africa) using finite rotations for the African motion in the Indo-Atlantic frame [*O'Neill et al.*, 2005, Table 2] and the GMHRF (Table 2). The resulting TPW paths are shown in Figures 10b and 10c, respectively.

[77] Both moving hot spot reference frames suggest a significant episode of TPW between 120 and 100 Ma, with faster angular rotation velocities during the 110–100 Ma interval (~0.8–1°/Ma), approximately aligned along the 100°E meridian. The GMHRF predicts a higher angular rate of the 110–100 Ma TPW episode (0.99°/Ma versus 0.79°/Ma in the Indo-Atlantic reference frame), which agrees well with an independent estimate of 1°/Ma obtained by *Steinberger and Torsvik* [2008] for this time interval from the analysis of coherent rotations of continental lithosphere in the paleomagnetic reference frame of *Torsvik et al.* [2008]. However, the axis of TPW rotation estimated by *Steinberger and Torsvik* [2008], which lies in the equatorial plane, passing through the 37.5°E meridian, is somewhat to the east of the position suggested by our reconstruction (~10°E, Figure 10c). Using the new global paleomagnetic compilation discussed above, *Torsvik et al.* [2012] revised their earlier TPW estimates [*Steinberger and Torsvik*, 2008], suggesting a 0.8°/Ma TPW rotation about an equatorial axis at 11°E during the 110–100 Ma interval. While the angular rate is ~0.2°/Ma slower than that estimated using the GMHRF, it is well within uncertainty limits of the latter (±0.7°/Ma at the nominal 95% confidence level). In contrast, the orientation of the TPW axis suggested by *Torsvik et al.* [2012] is now in excellent agreement with our estimate.

[78] For the 100–40 Ma interval, the two moving hot spot reference frames suggest disparate histories of TPW (Figures 10b and 10c). While minor TPW is observed in the Indo-Atlantic frame, the GMHRF suggests significant polar motion in Late Cretaceous to Eocene time, with the 90–60 Ma and 60–40 Ma segments of the TPW path forming a "hairpin" pattern of back-and-forth polar motion at average rates of 0.3°/Ma and 0.5°/Ma, respectively, which is nearly orthogonal to the early Cretaceous segment (120–100 Ma) and older segments identified by *Torsvik et al.* [2012]. Interestingly, the TPW estimates for the last 40 Ma (Figure 10c) indicate a slower, but nevertheless significant and systematic rotation of the Earth over the last 40 Ma (at an average rate of ~0.2°/Ma), about an axis similar to that suggested for the 120–100 Ma interval, which we consider to be not a mere coincidence.

[79] A recent study of *Steinberger and Torsvik* [2010] showed that the temporal variation of the Earth's non-hydrostatic inertia tensor can be successfully modeled by combining two major contributions, arising from (i) large low shear wave velocity provinces (LLSVPs) in the lowermost mantle and from (ii) subducted lithospheric slab material. Density anomalies associated with the LLSVPs largely control the orientation of the minimum axis of the non-hydrostatic inertia tensor. Reconstructions of large igneous provinces (LIPs), kimberlites and other intraplate igneous rocks considered to be sourced by mantle plumes consistently show that their locations, at the times when they have been erupted over the past 300 Ma, closely correlate with the edges of the African and Pacific LLSVPs [*Torsvik et al.*, 2006; *Burke et al.*, 2008; *Torsvik et al.*, 2008, 2010b]. These findings suggest that the igneous bodies have been created by deep plumes that rose from relatively narrow (~10°-wide) plume generation zones (PGZs) that surround the LLSVPs, directly above the CMB. An important implication is long-term longevity of the LLSVPs that appear to have existed and remained in their nearly present-day configuration since at least late Paleozoic time. Thus, if the LLSVPs solely controlled the orientation of the minimum axis of non-hydrostatic moment of inertia, we would expect TPW to be confined in a plane perpendicular to an axis that passes close to the centers of mass of the African LLSVP (15.6°S, 13°E), and of the Pacific LLSVP in the opposite hemisphere (11°S, 197.1°E) [*Steinberger and Torsvik*, 2008]. Remarkably, the 120–100 Ma and 40–0 Ma segments of the TPW path estimated using the GMHRF align parallel to the great circle drawn around the axis corresponding to the minimum moment of inertia of the combined masses of the two LLSVPs (Figure 11), which supports the dominant control of LLSVPs on the position of the TPW rotation axis during these time intervals. *Steinberger and Torsvik* [2010] showed that the opposite trends of TPW during 120–100 Ma and 40–0 Ma (120–50 Ma and 50–0 Ma according to their model) can be qualitatively explained by large amounts of subduction beneath North America during the Cretaceous time and by increased subduction beneath East Asia and South America, and a decrease beneath North America since the early Eocene (~50 Ma).

[80] Redistribution of mass due to sinking of lithospheric slabs changes the orientation of principal inertia axes through time, which may result in substantial departures from the "ideal" polar wandering confined to a plane perpendicular to the minimum inertia axis of the LLSVPs. It is encouraging that the numerical models of *Steinberger and Torsvik* [2010] were able to reproduce such deviations, with model TPW paths exhibiting turns and kinks that share many similarities with the TPW estimates obtained with the GMHRF (Figures 10c and 11). Specifically, a feature similar to the the 90–40 Ma hairpin is observed in the model TPW path of *Steinberger and Torsvik* [2010] for the 80–20 Ma interval, although it is less prominent and has an apex at 50 Ma, rather than 60 Ma. However, the TPW curve of *Steinberger and Torsvik* [2010] is substantially offset from that constructed using our moving hot spot reference frame. Thus, although we observe general qualitative agreement between our TPW

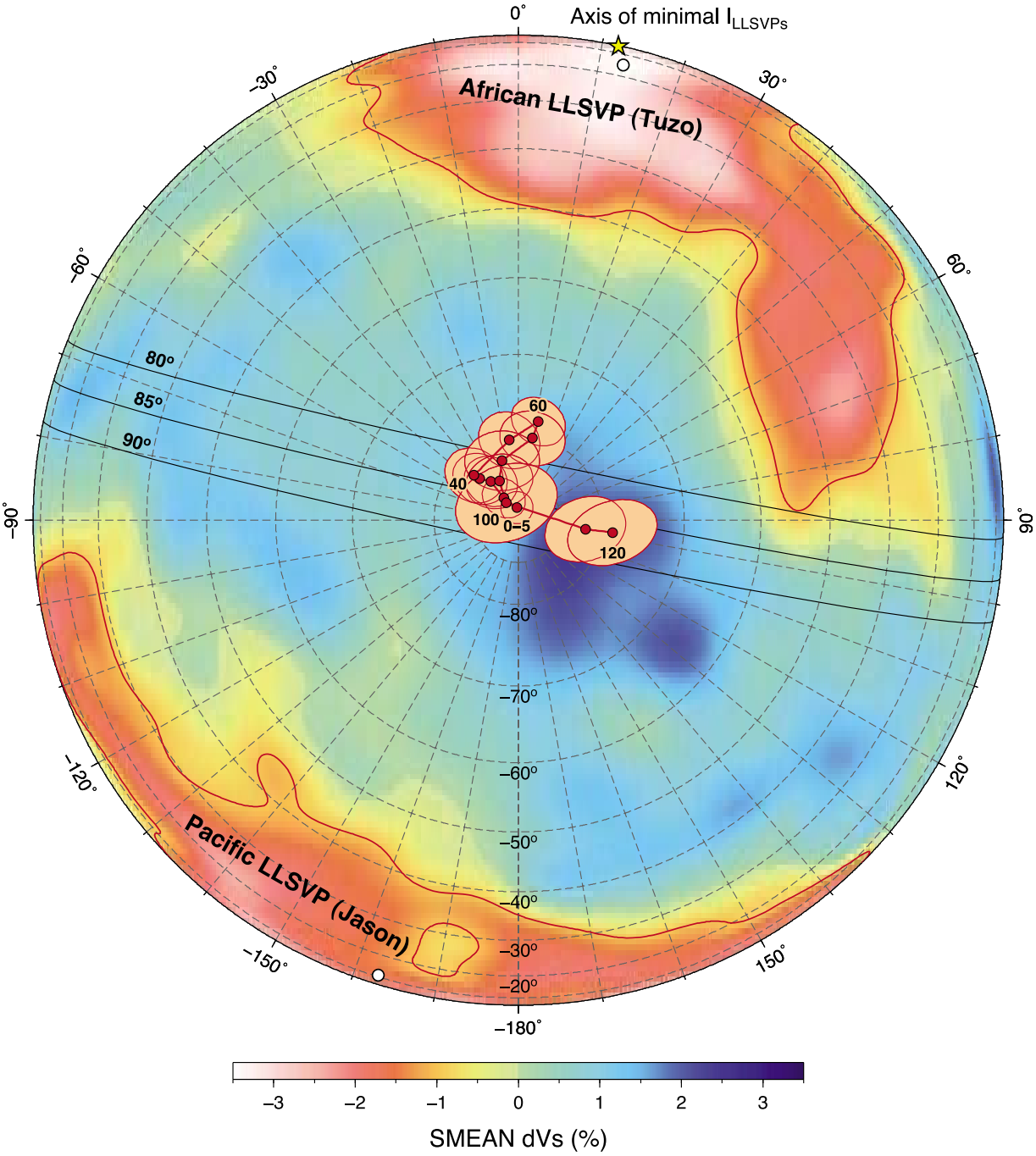

Figure 11. True polar wander path estimated using the GMHRF (Figure 10c) with respect to the African (Tuzo) and Pacific (Jason) LLSVPs in the lowermost mantle. The color map shows the variations of shear wave velocity (δV_s) at the lowest layer (2850 km depth) of the SMEAN tomographic model [*Becker and Boschi*, 2002]. Red lines are the −1% contours of δV_s corresponding to the steepest horizontal gradients and defining the edges of LLSVPs. White circles are the positions of centers of mass for the two LLSVPs; the yellow star corresponds to the axis of minimum moment of inertia for their combined masses [*Steinberger and Torsvik*, 2008]. Black lines show the 80°, 85° and 90° circles drawn around this axis.

estimates and results of the numerical model regarding the timing of changes, rates and directions of polar wander, it is by no means a good match.

[81] Considering that the model of *Steinberger and Torsvik* [2010] uses a simplified approach for estimating the variation of the inertia tensor through time by combining only the contributions from the stable LLSVPs and time-dependent subduction, and ignoring other possible contributions from hot upwellings, plumes and general advection of density anomalies in the mantle flow, this is an expected result. While it provides useful first-order predictions for TPW that successfully reproduce its general features, i.e., polar motion

predominantly along the great circle symmetric with respect to the LLSVPs changing in accord with variations in subduction zone geometries and slab sinking rates, the numerical model should be considered only as an approximation. We expect that further modeling efforts in the future will be able to produce more realistic histories of the changes in Earth's non-hydrostatic inertia tensor that could be directly compared to the TPW estimates based on the use of the global moving hot spot reference frame. In this regard, we note that the earlier work of *Steinberger and O'Connell* [1997, 2002], who modeled the redistribution of mantle density anomalies by backward advection but did not include the contributions from LLSVPs, produced estimates of TPW for the past 60 Ma that are in general agreement (in the sense of overall direction and rate) with those obtained using the GMHRF. This consistency suggests that modeling whole mantle convection, along with time-dependent subduction and stable LLSVP contributions, may be a key element in developing a comprehensive numerical treatment of TPW.

[82] Many tectonic events may have contributed to the development of the 90–60–40 Ma hairpin in the TPW path shown in Figure 10c. These could include the cessation of subduction and onset of spreading between the Pacific plate and Antarctica in the Late Cretaceous (~90 Ma), subduction of the Pacific-Izanagi ridge and demise of the Izanagi plate in Paleocene time (~60–55 Ma) [*Whittaker et al.*, 2007], initiation of subduction zones in the western Pacific and reorganization of the Pacific-Farallon spreading in the earliest Eocene, around 55 Ma [*Sharp and Clague*, 2006; *Tarduno*, 2007; *Atwater*, 1989], break-off of the Indian slab at the time of initial India-Asia collision (52 Ma) [*van Hinsbergen et al.*, 2011], and coupled changes in Indian and African absolute motion between 67 and 52 Ma, possibly triggered by arrival of the Deccan plume head [*Cande and Stegman*, 2011]. While all these events, and especially those associated with break-off of subducted slabs, have certainly played roles in changing the non-hydrostatic inertia tensor and corresponding rotations of the solid Earth with respect to the spin axis, establishing the causal links between TPW and its underlying dynamic triggers requires further and more comprehensive modeling work, which goes beyond the scope of our study. At this point, we feel it is premature to speculate on the exact causes of TPW in Late Cretaceous through early Eocene time.

6. Conclusions

[83] In this study, we have defined a new moving hot spot reference frame (GMHRF) that reconciles plate and plume motions in the Pacific, Atlantic and Indian oceans back to Early Cretaceous time (124 Ma). The reference frame is based on a global fit to hot spot tracks (i.e., using both the Pacific and Indo-Atlantic hot spots) back to the Late Cretaceous (80 Ma); for earlier reconstruction times it was defined using the Atlantic hot spots only. The GMHRF is a fully self-consistent model, implying that when the absolute plate motions are imposed as a boundary condition for estimating the variation in the mantle flow field through time, the numerical experiments on advection of plume conduits yield estimates of hot spot motion that are identical to those used to define the absolute plate kinematics.

[84] We demonstrated that when due care is taken in reconstructing the motion of the Pacific plate with respect to the plates of the Indo-Atlantic realm using a chain of relative plate motion through the Lord Howe Rise, Australia and East Antarctica, and when hot spot motions are quantified using the numerical models of the advection of plume conduits in the global mantle flow field, the fitted absolute rotations, combined with the estimates of hot spot drift, accurately reproduce the geometries and age progressions along tracks of the Pacific and Indo-Atlantic hot spots defining the GMHRF. Formal statistical tests for the goodness of model fit indicated no significant misfit for the entire reconstruction interval (0–124 Ma). The rotation uncertainties have been estimated from the errors assigned to the input data using a spherical regression algorithm and presented as covariance matrices [*Chang et al.*, 1990], which is the most common format for specifying rotation uncertainties in plate reconstructions.

[85] Fits of absolute kinematic solutions that incorporate estimates of hot spot motion were always superior compared to those in which hot spots were assumed fixed. Our attempts to define a global fixed hot spot reference frame have failed to produce acceptable fits to the segments of hot spot tracks formed from Late Cretaceous to Paleogene time (80–50 Ma). The formal statistical tests showed that the misfits in fixed hot spot reconstructions were highly significant, irrespective of the plate circuit model used to reconstruct the Pacific plate. This result highlights the importance of relative motion between the Pacific and Indo-Atlantic hot spots during the Late Cretaceous and Paleogene, once again supporting the earlier findings on hot spot mobility [*Molnar and Atwater*, 1973; *Stock and Molnar*, 1987; *Tarduno and Gee*, 1995; *Cande et al.*, 1995; *Tarduno and Cottrell*, 1997; *DiVenere and Kent*, 1999; *Raymond et al.*, 2000; *Tarduno et al.*, 2003; *Steinberger et al.*, 2004; *Doubrovine and Tarduno*, 2008a, 2008b]. We strongly argue that geoscientists should refrain from using or developing fixed hot spot reference frames.

[86] Compared to some earlier moving hot spot reconstructions, the kinematic model defined in this study implies significant revisions in the history of absolute plate motion in Late Cretaceous and Paleogene times (~90–50 Ma). Because of the large-scale differential motion between the Pacific and Indo-Atlantic hot spots during this interval, the Indo-Atlantic moving hot spot reconstructions of *O'Neill et al.* [2005] do not provide a reference frame that properly represents the entire Earth's mantle. Updated relative plate reconstructions, a new plate polygon model, and error analysis have been implemented in the GMHRF. Because of these updates, internal consistency and overall success in fitting hot spots tracks globally, the GMHRF supersedes our earlier moving hot spot frames [*Steinberger et al.*, 2004; *O'Neill et al.*, 2005; *Torsvik et al.*, 2008].

[87] One of the most important global implications of the new absolute plate motion model is the predicted amount of true polar wander, that is a rotation of the entire solid Earth with respect to the spin axis. Our estimates, obtained by transferring the synthetic apparent polar wander path of *Torsvik et al.* [2012] into the GMHRF, indicate two periods of TPW (120–100 Ma and 40–0 Ma) that was largely restricted to a plane perpendicular to the axis of minimum non-hydrostatic moment of inertia controlled by excess

masses of two nearly antipodal large low shear wave velocity provinces in the lowermost mantle, directly above the core-mantle boundary. The direction and rates of polar wander during these time intervals are consistent with the numerical results of *Steinberger and Torsvik* [2010], who modeled the changes of the Earth non-hydrostatic moment of inertia through time due to combined contributions of the stable LLSVPs and time-dependent subduction. The earlier (110–100 Ma) episode of relatively fast TPW (~1°/Ma) suggested by the GMHRF is in excellent agreement with the estimates obtained by *Steinberger and Torsvik* [2008] and *Torsvik et al.* [2012] from the analysis of coherent rotations of continents in a paleomagnetic reference frame; slow TPW with the opposite direction over the past 40 Ma was not detected in these studies. For 90–40 Ma, the GMHRF also predicts significant amounts of TPW at a 0.3–0.5°/Ma rate, about an axis that is nearly orthogonal to that suggested for the earlier and later times and with the opposite sense of rotation in the 90–60 Ma and 60–40 Ma time intervals, producing thus a "hairpin" feature in the TPW path with an apex at 60 Ma. We anticipate that numerical codes for modeling TPW will be improved in the near future to include whole-scale mantle convection, time-varying subduction and stable LLSVPs, allowing us to test whether this feature is feasible or not.

[88] In an effort to make our new GMHRF as useful for the geophysical community as possible, we list absolute plate rotations and their uncertainties for eight major lithospheric plates (African, Eurasian, Indian, Australian, East Antarctic, North American, South American and Pacific) in the auxiliary material Table S3. To facilitate future tests for the origin of intraplate volcanic features, we also included a supplementary data set that provides estimates of motion for the forty-four hot spots from the compilation of *Steinberger* [2000] (auxiliary material Data Set S1). Hot spot motions were modeled by advecting plume conduits in the mantle flow field corresponding to the final iteration of the GMHRF as described in section 2.3. The plume parameters used for these calculations [*Steinberger*, 2000; *Steinberger and Antretter*, 2006] are listed in auxiliary material Table S6. We note that many of the hot spots included in the list may not have a deep origin. Hence, the estimates presented in auxiliary material Data Set S1 should be treated with caution. Based on earlier studies [e.g., *Courtillot et al.*, 2003; *Ritsema and Allen*, 2003; *Montelli et al.*, 2004, 2006; *Torsvik et al.*, 2006] and recent numerical models [*Steinberger and Torsvik*, 2012], we suggest that in addition to Hawaii, Louisville, New England, Reunion and Tristan, twelve other hot spots (Azores, Canary, Cape Verde, Caroline, East Africa/Afar, Easter, Galapagos, Iceland, Kerguelen, Marion, Samoa and Yellowstone) have been sourced by plumes from the lower mantle. The origin of the remaining hot spots, more than 50% in the database, is debatable.

Appendix A: Spherical Regression Analysis—Definitions and Derivations

[89] Assume that the coeval locations from hot spot tracks have already been reconstructed relative to the anchor plate (section 2.2) and the hot spot positions at this reconstruction age have been estimated using the modeled plume motions (section 2.3). We will denote these locations as $\mathbf{u}_i$ and $\mathbf{v}_i$, respectively, where the index $i = 1, \ldots, n$ specifies a particular hot spot and its track, and n is the total number of tracks used in the reconstruction. Each $\mathbf{u}_i$ and $\mathbf{v}_i$ is to be written as a 3×1 column vector of an equal length, arbitrarily set to unity, $|\mathbf{u}_i| = |\mathbf{v}_i| = 1$. Both sets of vectors $\mathbf{u}_i$ and $\mathbf{v}_i$ are treated as independent random variables, which differ from their true unknown values $\mathbf{u}_{0i}$ and $\mathbf{v}_{0i}$ by small random errors $\delta\mathbf{u}_i$ and $\delta\mathbf{v}_i$, respectively,

$$\mathbf{u}_i = \mathbf{u}_{0i} + \delta\mathbf{u}_i \tag{A1}$$

$$\mathbf{v}_i = \mathbf{v}_{0i} + \delta\mathbf{v}_i \tag{A2}$$

and it is assumed that the $\mathbf{u}_{0i}$ and $\mathbf{v}_{0i}$ can be matched with an unknown rotation A_0, i.e.,

$$\mathbf{v}_{0i} = A_0\mathbf{u}_{0i} \tag{A3}$$

for all i. Note that defined this way, A_0 rotates track locations ($\mathbf{u}_i$) to their respective hot spots ($\mathbf{v}_i$), i.e., this is a finite reconstruction rotation for the absolute motion of the anchor plate.

[90] Since the observed $\mathbf{u}_i$ and $\mathbf{v}_i$ are perturbed by random variations, no exact fit between these two data sets is generally possible and the unknown rotation A_0 has to be estimated in the least squares sense, by finding a "best fit" rotation $\hat{A}$ that minimizes the misfit between the rotated set of points $\hat{A}\mathbf{u}_i$ and $\mathbf{v}_i$. The merit function for this regression problem is defined as the weighted sum of the squares of the misfits

$$\mathrm{SSE}(A) = \sum_{i=1}^{n} w_i|\mathbf{v}_i - A\mathbf{u}_i|^2 \tag{A4}$$

where weights w_i are inversely proportional to the variances of $\mathbf{v}_i - A\mathbf{u}_i$ and normalized so that

$$\sum_{i=1}^{n} w_i = n \tag{A5}$$

[91] The least squares estimate $\hat{A}$ is obtained by minimizing the SSE(A) over all possible candidate rotations A,

$$\mathrm{SSE}(\hat{A}) = \min\{\mathrm{SSE}(A)\} \tag{A6}$$

The analytical solution for this problem was derived by *Mackenzie* [1957], and can be computed as follows. First, we define a 3×3 matrix

$$X = U_n W V_n^{\mathrm{T}} \tag{A7}$$

where U_n and V_n are $3 \times n$ matrices whose columns are $\mathbf{u}_i$ and $\mathbf{v}_i$, respectively, and W is a diagonal $n \times n$ matrix composed of w_i/n, W = diag$\{w_i/n, \ldots, w_n/n\}$. Then, the matrix X is factorized using singular value decomposition into two orthogonal 3×3 matrices O_1 and O_2, and a diagonal matrix $\Lambda = \mathrm{diag}\{\lambda_1, \lambda_2, \lambda_3\}$ with non-negative elements ($\lambda_i \geq 0$ for $i = 1,2,3$),

$$X = O_1 \Lambda O_2^{\mathrm{T}} \tag{A8}$$

The best-fit rotation $\hat{A}$ is calculated using the equation

$$\hat{A} = O_2 O_1^{\mathrm{T}} \tag{A9}$$

[92] In the original treatment of *Chang* [1987], the errors of $\mathbf{u}_i$ and $\mathbf{v}_i$ were assumed identically distributed; hence, the regression weights were equal and arbitrarily set to unity ($w_i = 1$). Here we use a more general formulation (equation A4), allowing for the use of data with different quality. It can be proven that when the matrix X is defined by equation A7, the solutions obtained by *Chang* [1987] remain valid in the general case of unequal data variances.

[93] In our treatment of the rotation uncertainty, we consider a simple probability model, assuming that data errors are Fisherian, i.e. the probability density functions (PDFs) have the form

$$p(\mathbf{u}_i) = \frac{\kappa_{ui}}{4\pi \sinh \kappa_{ui}} \exp\left(\kappa_{ui}\mathbf{u}_i^{\mathrm{T}}\mathbf{u}_{0i}\right) \tag{A10}$$

$$p(\mathbf{v}_i) = \frac{\kappa_{vi}}{4\pi \sinh \kappa_{vi}} \exp\left(\kappa_{vi}\mathbf{v}_i^{\mathrm{T}}\mathbf{v}_{0i}\right) \tag{A11}$$

where κ_{ui} and κ_{vi} are the respective values of the concentration parameter. Noting that conceptually it might be more appropriate to assume elliptical uncertainties for the past hot spot locations [cf. *Andrews et al.*, 2006], we nevertheless chose to analyze Fisherian errors, because this significantly simplifies the treatment. From the analogy between Fisherian and circularly symmetric bivariate normal distributions discussed below, we suggest that the obtained results can be used in a more general case of normally distributed "elliptical" errors. Yet, we cannot validate such generalization with a rigorous proof.

[94] In plate tectonic applications, the errors are small compared to the radius of the sphere, and distributions are highly concentrated around the mean values ($\kappa_{ui} \gg 1$ and $\kappa_{vi} \gg 1$ for all i). When κ is large, a Fisherian distribution can be approximated by a bivariate normal distribution,

$$p(\mathbf{u}_i) = \frac{1}{2\pi\sigma_{ui}^2} \exp\left(-\frac{(\mathbf{u}_i - \mathbf{u}_{0i})^2}{2\sigma_{ui}^2}\right) \tag{A12}$$

with the one-dimensional variance $\sigma_{vi}^2 = 1/\kappa_{ui}$ (expressed in squared radians), and similarly for the $\mathbf{v}_i$. By analogy with a convolution of two normal distributions, the distribution of $\mathbf{v}_i - A_0\mathbf{u}_i$ is also approximately normal

$$p(\mathbf{v}_i - A_0\mathbf{u}_i) = \frac{1}{2\pi\sigma_i^2} \exp\left(-\frac{(\mathbf{v}_i - A_0\mathbf{u}_i)^2}{2\sigma_i^2}\right) \tag{A13}$$

with the zero mean and variance

$$\sigma_i^2 = \sigma_{ui}^2 + \sigma_{vi}^2 = \frac{\kappa_{ui} + \kappa_{vi}}{\kappa_{ui}\kappa_{vi}} \tag{A14}$$

Because the 2D variance of $\mathbf{v}_i - A_0\mathbf{u}_i$ is $2\sigma_i^2$, the regression weights can be expressed as

$$w_i = \frac{\sigma^2}{\sigma_i^2} \tag{A15}$$

where σ^2 is the average combined data variance defined by the equation

$$\frac{1}{\sigma^2} = \frac{1}{n}\sum_{i=1}^{n}\frac{1}{\sigma_i^2} \tag{A16}$$

[95] The confidence region for the unknown rotation A_0 is estimated from the uncertainties of data ($\mathbf{u}_i$, $\mathbf{v}_i$). Parameterizing the rotations in the vicinity of A_0 as

$$\hat{A} = A_0\Phi(\mathbf{h}) \tag{A17}$$

where $\Phi(\mathbf{h})$ is a small, right-hand rule rotation about vector $\mathbf{h}$ by $|\mathbf{h}|$ radians [*Chang et al.*, 1990], expanding $\Phi(\mathbf{h})$ into the exponential series and retaining only the linear term, the perturbing rotation $\Phi(\mathbf{h})$ is approximated by

$$\Phi(\mathbf{h}) = \sum_{k=0}^{\infty}\frac{M(\mathbf{h})^k}{k!} \approx I + M(\mathbf{h}) \tag{A18}$$

where I is the identity matrix and $M(\mathbf{h})$ is a skew-symmetric matrix composed of the elements of $\mathbf{h} = (h_1, h_2, h_3)^{\mathrm{T}}$

$$M(\mathbf{h}) = \begin{pmatrix} 0 & -h_3 & h_2 \\ h_3 & 0 & -h_1 \\ -h_2 & h_1 & 0 \end{pmatrix} \tag{A19}$$

This approximation is then used to estimate the covariance matrix of $\mathbf{h}$ in a way analogous to standard nonlinear regression [*Chang*, 1986, 1987]

$$\mathrm{cov}(\mathbf{h}) = \frac{1}{\kappa n}\left(I - \hat{\Sigma}\right)^{-1} \tag{A20}$$

where $\kappa = 1/\sigma^2$, and

$$\hat{\Sigma} = \frac{X\hat{A}}{(\coth 2\kappa - 1/2\kappa)^2} \tag{A21}$$

The confidence region for A_0 at an α significance level (typically, α = 5% to produce a 95% confidence region) is defined by all rotations $A = \hat{A}\Phi(\mathbf{h})$ with $\mathbf{h}$ satisfying the condition

$$\mathbf{h}^{\mathrm{T}}\mathrm{cov}(\mathbf{h})^{-1}\mathbf{h} = n\kappa\mathbf{h}^{\mathrm{T}}\left(I - \hat{\Sigma}\right)\mathbf{h} \le \chi_\alpha^2[3] \tag{A22}$$

where $\chi_\alpha^2[3]$ is the upper critical value of the χ^2 distribution with 3 degrees of freedom. It also follows that $\mathrm{SSE}(\hat{A})/\sigma^2$ is distributed as $\chi^2[2n - 3]$, which provides a formal statistical test for the goodness of fit. Assuming that the data errors are correct, the value

$$\chi^2 = \frac{\mathrm{SSE}(\hat{A})}{\sigma^2} \le \chi_\alpha^2[2n - 3] \tag{A23}$$

indicates that the observed misfit between $\mathbf{v}_i$ and $\hat{A}\mathbf{u}_i$ is acceptable, i.e., the fitted rotation $\hat{A}$ reconstructs the two sets of spherical data with a small misfit, which is within the limit expected from the uncertainties of the data at the significance level α.

[96] **Acknowledgments.** This study contributes to the TOPO-4D collaborative research project of the TOPO-EUROPE program organized by the European Science Foundation. P.D. and T.H.T. are grateful for financial support from the Norwegian Research Council (Mantle Forcing: grant 195911), Statoil (Akademiavtalen), and the European Research Council under the European Union's Seventh Framework Programme (FP7/2007–2013), ERC advanced grant agreement 267631 (Beyond Plate Tectonics). The authors greatly appreciate the hospitality and financial support provided by the Centre for Advanced Study at the Norwegian Academy of Science

and Letters, who hosted our research group from August 2010 to June 2011. We would like to thank Kevin Burke, Carmen Gaina, Douwe van Hinsbergen, and Wim Spakman for comments and discussions. We thank R. Dietmar Müller, an anonymous reviewer, and an anonymous Associate Editor who provided helpful and constructive reviews of the manuscript.

References

Acton, G. D., and R. G. Gordon (1994), Paleomagnetic tests of the Pacific plate reconstructions and implications for motion between the hot spots, *Science*, *263*, 1246–1254.

Andrews, D. L., R. G. Gordon, and B. C. Horner-Johnson (2006), Uncertainties in plate reconstructions relative to the hot spots: Pacific-hot spot rotations and uncertainties for the past 68 million years, *Geophys. J. Int.*, *166*, 939–951, doi:10.1111/j.1365-246X.2006.03029.x.

Atwater, T. (1989), Plate tectonic history of the northeast Pacific and western North America, in *The Geology of North America*, vol. N, *The Eastern Pacific Ocean and Hawaii*, edited by E. L. Winterer et al., pp. 21–72, Geol. Soc. of Am., Boulder, Colo.

Becker, T. W. (2006), On the effect of temperature and strain-rate dependent viscosity on global mantle flow, net rotation, and plate-driving forces, *Geophys. J. Int.*, *167*(2), 943–957, doi:10.1111/j.1365-246X.2006.03172.x.

Becker, T. W., and L. Boschi (2002), A comparison of tomographic and geodynamic mantle models, *Geochem. Geophys. Geosyst.*, *3*(1), 1003, doi:10.1029/2001GC000168.

Bernard, A., M. Munschy, Y. Rotstein, and D. Sauter (2005), Refined spreading history at the Southwest Indian Ridge for the last 96 Ma, with the aid of satellite gravity data, *Geophys. J. Int.*, *162*, 765–778, doi:10.1111/j.1365-246X.2005.02672.x.

Besse, J., and V. Courtillot (2002), Apparent and true polar wander and the geometry of geomagnetic field over the last 250 Myr, *J. Geophys. Res.*, *107*(B11), 2300, doi:10.1029/2000JB000050.

Burke, K., B. Steinberger, T. H. Torsvik, and M. A. Smethurst (2008), Plume generation zones at the margins of large low shear velocity provinces on the core–mantle boundary, *Earth Planet. Sci. Lett.*, *265*, 49–60, doi:10.1016/j.epsl.2007.09.042.

Cande, S. C., and D. V. Kent (1995), Revised calibration of the geomagnetic polarity timescale for the Late Cretaceous and Cenozoic, *J. Geophys. Res.*, *100*(B4), 6093–6095.

Cande, S. C., and D. R. Stegman (2011), Indian and African plate motions driven by the push force of the Reunion plume head, *Nature*, *475*, 47–52, doi:10.1038/nature10174.

Cande, S. C., and J. M. Stock (2004a), Pacific-Antarctic-Australia motion and the formation of the Macquarrie plate, *Geophys. J. Int.*, *157*, 399–414.

Cande, S. C., and J. M. Stock (2004b), Cenozoic reconstructions of the Australia-New Zealand-South Pacific sector of Antarctica, in *The Cenozoic Southern Ocean: Tectonics, Sedimentation and Climate Change Between Australia and Antarctica*, *Geophys. Monogr. Ser.*, vol. 151, edited by N. F. Exon et al., pp. 5–17, AGU, Washington, D. C.

Cande, S. C., C. A. Raymond, J. Stock, and W. F. Haxby (1995), Geophysics of the Pitman Fracture Zone and Pacific-Antarctic plate motions during the Cenozoic, *Science*, *270*, 947–953.

Cande, S. C., J. Stock, R. D. Müller, and T. Ishihara (2000), Cenozoic motion between East and West Antarctica, *Nature*, *404*, 145–150.

Cande, S. C., P. Patriat, and J. Dyment (2010), Motion between the Indian, Antarctic and African plates in the early Cenozoic, *Geophys. J. Int.*, *183*, 127–149, doi:10.1111/j.1365-246X.2010.04737.x.

Chandler, M. T., P. Wessel, B. Taylor, M. Seton, S.-S. Kim, and K. Hyeong (2012), Reconstructing Ontong Java Nui: Implications for Pacific absolute plate motion, hot spot drift and true polar wander, *Earth Planet. Sci. Lett.*, *331–332*, 140–151, doi:10.1016/j.epsl.2012.03.017.

Chang, T. (1986), Spherical regression, *Ann. Stat.*, *14*(3), 907–924.

Chang, T. (1987), On the statistical properties of estimated rotations, *J. Geophys. Res.*, *92*(B7), 6319–6329.

Chang, T. (1988), Estimating the relative rotation of two tectonic plates from boundary crossings, *J. Am. Stat. Assoc.*, *83*(404), 1178–1183.

Chang, T., J. Stock, and P. Molnar (1990), The rotation group in plate tectonics and the representation of uncertainties of plate reconstructions, *Geophys. J. Int.*, *101*, 649–661.

Chu, D., and R. G. Gordon (1999), Evidence for motion between Nubia and Somalia along the Southwest Indian ridge, *Nature*, *398*, 64–67.

Conrad, C. P., and M. D. Behn (2010), Constraints on lithosphere net rotation and asthenospheric viscosity from global mantle flow models and seismic anisotropy, *Geochem. Geophys. Geosyst.*, *11*, Q05W05, doi:10.1029/2009GC002970.

Conrad, C. P., and M. Gurnis (2003), Seismic tomography, surface uplift, and the breakup of Gondwanaland: Integrating mantle convection backwards in time, *Geochem. Geophys. Geosyst.*, *4*(3), 1031, doi:10.1029/2001GC000299.

Courtillot, V., and J. Besse (2004), A long-term octupolar component of the geomagnetic field? (0–200 million years B.P.), in *Timescales of the Paleomagnetic Field*, *Geophys. Monogr. Ser.*, vol. 145, edited by J. E. T. Channel et al., pp. 59–74, AGU, Washington, D. C.

Courtillot, V., A. Davaille, J. Besse, and J. M. Stock (2003), Three distinct types of hot spots in the Earth's mantle, *Earth Planet. Sci. Lett.*, *205*, 295–308.

Croon, M. B., S. C. Cande, and J. M. Stock (2008), Revised Pacific-Antarctic plate motions and geophysics of the Menard Fracture Zone, *Geochem. Geophys. Geosyst.*, *9*, Q07001, doi:10.1029/2008GC002019.

Davis, A. S., L. B. Gray, D. A. Clague, and J. R. Hein (2002), The Line Islands revisited: New $^{40}Ar/^{39}Ar$ geochronologic evidence for episodes of volcanism due to lithospheric extension, *Geochem. Geophys. Geosyst.*, *3*(3), 1018, doi:10.1029/2001GC000190.

DeMets, C., R. G. Gordon, and J.-Y. Royer (2005), Motion between the Indian, Capricorn and Somalian plates since 20 Ma: implications for the timing and magnitude of distributed lithospheric deformation in the equatorial Indian Ocean, *Geophys. J. Int.*, *161*, 445–468, doi:10.1111/j.1365-246X.2005.02598.x.

DiVenere, V., and D. V. Kent (1999), Are the Pacific and Indo-Atlantic hot spots fixed? Testing the plate circuit though Antarctica, *Earth Planet. Sci. Lett.*, *170*, 105–117.

Doubrovine, P. V., and J. A. Tarduno (2004), Late Cretaceous paleolatitude of the Hawaiian Hot Spot: New paleomagnetic data from Detroit Seamount (ODP Site 883), *Geochem. Geophys. Geosyst.*, *5*, Q11L04, doi:10.1029/2004GC000745.

Doubrovine, P. V., and J. A. Tarduno (2008a), Linking the Late Cretaceous to Paleogene Pacific plate and the Atlantic bordering continents using plate circuits and paleomagnetic data, *J. Geophys. Res.*, *113*, B07104, doi:10.1029/2008JB005584.

Doubrovine, P. V., and J. A. Tarduno (2008b), A revised kinematic model for the relative motion between Pacific oceanic plates and North America since the Late Cretaceous, *J. Geophys. Res.*, *113*, B12101, doi:10.1029/2008JB005585.

Doubrovine, P. V., J. A. Tarduno, and X. Zhao (2009), On the magnetostratigraphic age of Nauru Basin basalts of the western Pacific Ocean and timing of Ontong Java volcanism, *Earth Planet. Sci. Lett.*, *287*, 175–184, doi:10.1016/j.epsl.2009.07.040.

Duncan, R. A. (1981), Hot spots in the southern oceans—An absolute frame of reference for motion of the Gondwana continents, *Tectonophysics*, *74*, 29–42.

Duncan, R. A., and D. A. Clague (1985), Pacific plate motion recorded by linear volcanic chains, in *The Ocean Basins and Margins*, vol. 7A, *The Pacific Ocean*, edited by A. E. A. Nairn et al., pp. 89–121, Plenum, New York.

Duncan R. A., and R. A. Keller (2004), Radiometric ages for basement rocks from the Emperor Seamounts, ODP Leg 197, *Geochem. Geophys. Geosyst.*, *5*, Q08L03, doi:10.1029/2004GC000704.

Dziewonski, A. M., and D. L. Anderson (1981), Preliminary Reference Earth Model, *Phys. Earth Planet. Inter.*, *25*, 297–356.

Engebretson, D. C., A. Cox, and R. G. Gordon (1985), Relative motions between oceanic and continental plates in the Pacific basin, *Spec. Pap. Geol. Soc. Am.*, *206*, 59 pp.

Gaina, C., D. R. Müller, J.-Y. Royer, J. Stock, J. Hardebeck, and P. Symonds (1998), The tectonic history of the Tasman Sea: A puzzle with 13 pieces, *J. Geophys. Res.*, *103*, 12,413–12,433.

Goldreich, P., and A. Toomre (1969), Some remarks on polar wandering, *J. Geophys. Res.*, *74*, 2555–2567.

Gradstein, F. M., F. P. Agterberg, J. G. Ogg, J. Hardenbol, P. van Veen, J. Thierry, and Z. Huang (1994), A Mesozoic time scale, *J. Geophys. Res.*, *99*(B12), 24,051–24,074.

Hager, B. H., and R. J. O'Connell (1979), Kinematic models of large-scale flow in the Earth's mantle, *J. Geophys. Res.*, *84*(B3), 1031–1048.

Hager, B. H., and R. J. O'Connell (1981), A simple global model of plate dynamics and mantle convection, *J. Geophys. Res.*, *86*(B6), 4843–4867.

Harada, Y., and Y. Hamano (2000), Recent progress on plate motions relative to hot spots, in *The History and Dynamics of Global Plate Motions*, *Geophys. Monogr. Ser.*, vol. 121, edited by M. A. Richards, R. G. Gordon, and R. D. van der Hilst, pp. 327–338, AGU, Washington, D. C.

Hellinger, S. J. (1981), The uncertainties of finite rotations in plate tectonics, *J. Geophys. Res.*, *86*(B10), 9312–9318.

Horner-Johnson, B. C., R. G. Gordon, and D. F. Argus (2007), Plate kinematic evidence for the existence of a distinct plate between the Nubian and Somalian plates along the Southwest Indian Ridge, *J. Geophys. Res.*, *112*, B05418, doi:10.1029/2006JB004519.

Jupp, P. E., and J. T. Kent (1987), Fitting smooth paths to spherical data *Appl. Stat.*, *36*, 34–46.

Koppers, A. A. P., H. Staudigel, J. R. Wijbrans, and M. S. Pringle (1998), The Magellan seamount trail: Implications for Cretaceous hot spot volcanism and absolute Pacific plate motion, *Earth Planet. Sci. Lett.*, *163*, 53–68.

Koppers, A. A. P., J. P. Morgan, J. W. Morgan, and H. Staudigel (2001), Testing the fixed hot spot hypothesis using $^{40}Ar/^{39}Ar$ age progressions along seamount trails, *Earth Planet. Sci. Lett.*, *185*, 237–252.

Koppers, A. A. P., R. A. Duncan, and B. Steinberger (2004), Implications of a nonlinear $^{40}Ar/^{39}Ar$ age progression along the Louisville seamount trail for models of fixed and moving hot spots, *Geochem. Geophys. Geosyst.*, *5*, Q06L02, doi:10.1029/2003GC000671.

Koppers, A. A. P., M. D. Gowen, L. E. Colwell, J. S. Gee, P. F. Lonsdale, J. J. Mahoney, and R. A. Duncan (2011), New $^{40}Ar/^{39}Ar$ age progression for the Louisville hot spot trail and implications for inter-hot spot motion, *Geochem. Geophys. Geosyst.*, *12*, Q0AM02, doi:10.1029/2011GC003804.

Larter, R. D., A. P. Cunningham, P. F. Barker, K. Gohl, and F. O. Nitsche (2002), Tectonic evolution of the Pacific margin of Antarctica: 1. Late Cretaceous tectonic reconstructions, *J. Geophys. Res.*, *107*(B12), 2345, doi:10.1029/2000JB000052.

Lemaux, J., R. G. Gordon, and J.-Y. Royer (2002), Location of the Nubia-Somalia boundary along the Southwest Indian Ridge, *Geology*, *30*, 339–342.

Lonsdale, P. (1988), Paleogene history of the Kula plate: Offshore evidence and onshore implications, *Geol. Soc. Am. Bull.*, *100*, 733–754.

Mackenzie, J. K. (1957), The estimation of orientation relationship, *Acta Cryst.*, *10*, 61–62.

McElhinny, M. W. (2004), Geocentric axial dipole hypothesis: A least squares perspective, in *Timescales of the Paleomagnetic Field*, *Geophys. Monogr. Ser.*, vol. 145, edited by J. E. T. Channel et al., pp. 1–12, AGU, Washington, D. C.

McElhinny, M. W., P. L. McFadden, and R. T. Merrill (1996), Time-averaged paleomagnetic field 0–5 Ma, *J. Geophys. Res.*, *101*, 25,007–25,027.

McKenzie, D. P., and R. L. Parker (1967), The north Pacific: An example of tectonics on a sphere, *Nature*, *216*, 1276–1280.

Merkouriev, S., and C. DeMets (2006), Constraints on Indian plate motion since 20 Ma from dense Russian magnetic data: Implications for Indian plate dynamics, *Geochem. Geophys. Geosyst.*, *7*, Q02002, doi:10.1029/2005GC001079.

Mihalffy, P., B. Steinberger, and H. Schmeling (2008), The effect of the large-scale mantle flow field on the Iceland hot spot track, *Tectonophysics*, *447*, 5–18, doi:10.1016/j.tecto.2006.12.012.

Molnar, P., and T. Atwater (1973), Relative motion of hot spots in the mantle, *Nature*, *246*, 288–291.

Molnar, P., and J. M. Stock (1987), Relative motion of hot spots in the Pacific, Atlantic and Indian oceans since late Cretaceous time, *Nature*, *327*, 587–591.

Molnar, P., and J. M. Stock (2009), Slowing of India's convergence with Eurasia since 20 Ma and its implications for Tibetan mantle dynamics, *Tectonics*, *28*, TC3001, doi:10.1029/2008TC002271.

Molnar, P., F. Pardo-Casas, and J. Stock (1988), The Cenozoic and Late Cretaceous evolution of the Indian Ocean Basin: Uncertainties in the reconstructed positions of the Indian, African and Antarctic plates, *Basin Res.*, *1*, 23–40.

Montelli, R., G. Nolet, F. A. Dahlen, G. Masters, E. R. Engdahl, and S.-H. Hung (2004), Finite frequency tomography reveals a variety of mantle plumes, *Science*, *303*, 338–343.

Montelli, R., G. Nolet, F. A. Dahlen, and G. Masters (2006), A catalogue of deep mantle plumes: New results from finite-frequency tomography, *Geochem. Geophys. Geosyst.*, *7*, Q11007, doi:10.1029/2006GC001248.

Morgan, W. J. (1968), Rises, trenches, great faults, and crustal blocks, *J. Geophys. Res.*, *73*(6), 1959–1982.

Morgan, W. J. (1971), Convection plumes in the lower mantle, *Nature*, *230*, 42–43.

Morgan, W. J. (1981), Hot spot tracks and the opening of the Atlantic and Indian oceans, in *The Sea*, vol. 7, *The Oceanic Lithosphere*, edited by C. Emiliani et al., pp. 443–487, Wiley Intersci., New York.

Müller, R. D., J.-Y. Royer, and L. A. Lawver (1993), Revised plate motions relative to hot spots from combined Atlantic and Indian Ocean hot spot tracks, *Geology*, *21*, 275–278.

O'Neill, C., R. D. Müller, and B. Steinberger (2005), On the uncertainties in hot spot reconstructions and the significance of moving hot spot reference frames, *Geochem. Geophys. Geosyst.*, *6*, Q04003, doi:10.1029/2004GC000784.

Raymond, C. A., J. M. Stock, and S. C. Cande (2000), Fast Paleogene motion of the Pacific hot spots from revised global plate circuit constraints, in *The History and Dynamics of Global Plate Motion*, *Geophys. Monogr. Ser.*, vol. 121, edited by M. A. Richards et al., pp. 359–375, AGU, Washington, D. C.

Ritsema, J., and R. M. Allen (2003), The elusive mantle plume, *Earth Planet. Sci. Lett.*, *207*, 1–12.

Royer, J.-Y., and T. Chang (1991), Evidence for relative motion between the Indian and Australian plates during the last 20 m.y. from Pacific tectonic reconstructions: Implications for the deformation of the Indo-Australian plate, *J. Geophys. Res.*, *96*, 11,779–11,802.

Sandwell, D. T., and W. H. F. Smith (1997), Marine gravity anomaly from Geosat and ERS 1 satellite altimetry, *J. Geophys. Res.*, *102*, 10,039–10,054.

Sharp, W. D., and D. A. Clague (2006), 50-Ma initiation of Hawaiian-Emperor bend records major change in Pacific plate motion, *Science*, *313*, 1281–1284.

Steinberger, B. (2000), Plumes in a convecting mantle: Models and observations from individual hot spots, *J. Geophys. Res.*, *105*(B5), 11,127–11,152.

Steinberger, B., and M. Antretter (2006), Conduit diameter and buoyant rising speed of mantle plumes: Implications for the motion of hot spots and shape of plume conduits, *Geochem. Geophys. Geosyst.*, *7*, Q11018, doi:10.1029/2006GC001409.

Steinberger, B., and A. R. Calderwood (2006), Models of large-scale viscous flow in the Earth's mantle with constraints from mineral physics and surface observations, *Geophys. J. Int.*, *167*, 1461–1481, doi:10.1111/j.1365-246X.2006.03131.x.

Steinberger, B., and C. Gaina (2007), Plate-tectonic reconstructions predict part of the Hawaiian hot spot track to be preserved in the Bering Sea, *Geology*, *35* (5), 407–410, doi:10.1130/G23383A.1.

Steinberger, B., and R. J. O'Connell (1997), Changes of the Earth's rotation axis owing to advection of mantle density heterogeneities, *Nature*, *387*, 169–173.

Steinberger, B., and R. J. O'Connell (1998), Advection of plumes in mantle flow: Implications for hot spot motion, mantle viscosity and plume distribution, *Geophys. J. Int.*, *132*, 412–434.

Steinberger, B., and R. J. O'Connell (2002), The convective mantle flow signal in rates of true polar wander, in *Ice Sheets, Sea Level and the Dynamic Earth*, *Geodyn. Ser.*, vol. 29, edited by J. X. Mitrovica and L. L. A. Vermeersen, pp. 233–256, AGU, Washington, D. C.

Steinberger, B., and T. H. Torsvik (2008), Absolute plate motions and true polar wander in the absence of hot spot tracks, *Nature*, *452*, 620–623, doi:10.1038/nature06824.

Steinberger, B., and T. H. Torsvik (2010), Toward an explanation for the present and past locations of the poles, *Geochem. Geophys. Geosyst.*, *11*, Q06W06, doi:10.1029/2009GC002889.

Steinberger, B., and T. H. Torsvik (2012), A geodynamic model of plumes from the margins of Large Low Shear Velocity Provinces, *Geochem. Geophys. Geosyst.*, *13*, Q01W09, doi:10.1029/2011GC003808.

Steinberger, B., R. Sutherland, and R. J. O'Connell (2004), Prediction of Hawaiian-Emperor seamount locations from a revised model of global plate motion and mantle flow, *Science*, *430*, 167–173.

Stock, J. M., and P. Molnar (1987), Revised history of early Tertiary plate motion in the south–west Pacific, *Nature*, *325*, 495–499.

Stock, J. M., and P. Molnar (1988), Uncertainties and implications of the Late Cretaceous and Tertiary position of North America relative to the Farallon, Kula and Pacific plates, *Tectonics*, *7*, 1339–1384.

Sutherland, R. (1995), The Australia-Pacific boundary and Cenozoic plate motion in the SW Pacific: Some constraints from Geosat data, *Tectonics*, *14*, 819–831.

Tarduno, J. A. (2007), On the motion of Hawaii and other mantle plumes, *Chem. Geol.*, *241*, 234–247.

Tarduno, J. A., and R. D. Cottrell (1997), Paleomagnetic evidence for motion of the Hawaiian hot spot during formation of the Emperor seamounts, *Earth Planet. Sci. Lett.*, *153*, 171–180.

Tarduno, J. A., and J. Gee (1995), Large-scale motion between Pacific and Atlantic hot spots, *Nature*, *378*, 477–480.

Tarduno, J. A., R. D. Cottrell, and A. V. Smirnov (2002), The Cretaceous superchron geodynamo: Observations near the tangent cylinder, *Proc. Natl. Acad. Sci. U. S. A.*, *99*(22), 14020–14025.

Tarduno, J. A., R. A. Duncan, D. W. Scholl, R. D. Cottrell, B. Steinberger, T. Thordarson, B. C. Kerr, C. R. Neal, M. Torii, and C. Carvallo (2003), The Emperor Seamounts: Southward motion of the Hawaiian hot spot plume in Earth's mantle, *Science*, *301*, 1064–1069.

Tarduno, J. A., H.-P. Bunge, N. Sleep, and U. Hansen (2009), The bent Hawaiian-Emperor hot spot track: Inheriting the mantle wind, *Science*, *324*, 50–53, doi:10.1126/science.1161256.

Taylor, B. (2006), The single largest oceanic plateau: Ontong Java-Manihiki-Hikurangi, *Earth Planet. Sci. Lett.*, *241*, 372–380, doi:10.1016/j.epsl.2005.11.049.

Tikku, A. A., and S. C. Cande (2000), On the fit of Broken Ridge and Kerguelen Plateau, *Earth Planet. Sci Lett.*, *180*, 117–132.

Tikku, A. A., and N. G. Direen (2008), Comment on "Major Australian-Antarctic plate reorganization at Hawaiian-Emperor bend time," *Science*, *321*, 490.

Torsvik, T. H., R. Van der Voo, J. G. Meert, J. Mosar, and H. J. Walderhaug (2001), Reconstructions of the continents around the North Atlantic at about the 60th parallel, *Earth Planet. Sci. Lett.*, *187*, 55–69.

Torsvik, T. H., M. A. Smethurst, K. Burke, and B. Steinberger (2006), Large igneous provinces generated from the margins of the large low-velocity provinces in the deep mantle, *Geophys. J. Int.*, *167*, 1447–1460.

Torsvik, T. H., R. D. Müller, R. Van der Voo, B. Steinberger, and C. Gaina (2008), Global plate motion frames: Toward a unified model, *Rev. Geophys.*, *46*, RG3004, doi:10.1029/2007RG000227.

Torsvik, T. H., B. Steinberger, M. Gurnis, and C. Gaina (2010a), Plate tectonics and net lithosphere rotation over the past 150 My, *Earth Planet. Sci. Lett.*, *291*, 106–112, doi:10.1016/j.epsl.2009.12.055.

Torsvik, T. H., K. Burke, B. Steinberger, S. J. Webb, and L. D. Ashwal (2010b), Diamonds sampled by plumes from the core-mantle boundary, *Nature*, *466*, 352–355, doi:10.1038/nature09216.

Torsvik, T. H., et al. (2012), Phanerozoic polar wander and palaeogeography and dynamics, *Earth Sci. Rev.*, *114*, 325–368, doi:10.1016/j.earscirev.2012.06.007.

Tucholke, B. E., and N. C. Smoot (1990), Evidence for age and evolution of Corner Seamounts and Great Meteor Seamount chain from multibeam bathymetry, *J. Geophys. Res.*, *95*(B11), 17,555–17,569.

van der Meer, D. G., W. Spakman, D. J. J. van Hinsbergen, M. L. Amaru, and T. H. Torsvik (2010), Towards absolute plate motions constrained by lower-mantle slab remnants, *Nat. Geosci.*, *3*, 36–40, doi:10.1038/NGEO708.

van Fossen, M. C., and D. V. Kent (1992), Paleomagnetism of 122 Ma plutons in New England and the mid-Cretaceous paleomagnetic field in North America: True polar wander or large-scale differential mantle motion?, *J. Geophys. Res.*, *97*(B13), 19,651–19,661.

van Hinsbergen, D. J. J., B. Steinberger, P. V. Doubrovine, and R. Gassmöller (2011), Acceleration and deceleration of India-Asia convergence since the Cretaceous: Roles of mantle plumes and continental collision, *J. Geophys. Res.*, *116*, B06101, doi:10.1029/2010JB008051.

Wessel, P., and L. W. Kroenke (1997), A geometric technique for relocating hot spots and refining absolute plate motions, *Nature*, *387*, 365–369.

Wessel, P., and L. Kroenke (2008), Pacific absolute plate motion since 145 Ma: An assessment of the fixed hot spot hypothesis, *J. Geophys. Res.*, *113*, B06101, doi:10.1029/2007JB005499.

Wessel, P., and L. W. Kroenke (2009), Observations of geometry and ages constrain relative motion of Hawaii and Louisville plumes, *Earth Planet. Sci. Lett.*, *284*, 467–472, doi:10.1016/j.epsl.2009.05.012.

Wessel, P., Y. Harada, and L. W. Kroenke (2006), Toward a self-consistent, high-resolution absolute plate motion model for the Pacific, *Geochem. Geophys. Geosyst.*, *7*, Q03L12, doi:10.1029/2005GC001000.

Whittaker, J. M., R. D. Müller, G. Leitchenkov, H. Stagg, M. Sdrolias, C. Gaina, and A. Goncharov (2007), Major Australian-Antarctic plate reorganization at Hawaiian-Emperor Bend time, *Science*, *318*, 83–86.

Whittaker, J., S. Williams, N. Kusznir, and R. D. Müller (2010), Restoring the continent-ocean boundary: Constraints from lithospheric stretching grids and tectonic reconstructions, paper presented at ASEG-PESA 21st International Geophysical Conference, Sydney, Australia.

Williams, S. E., J. M. Whittaker, and R. D. Müller (2011), Full-fit, palinspastic reconstruction of the conjugate Australian-Antarctic margins, *Tectonics*, *30*, TC6012, doi:10.1029/2011TC002912.

Wilson, J. T. (1963), Hypothesis of Earth's behaviour, *Nature*, *198*, 925–929.